EROSIONAL AND DEPOSITIONAL PROCESSES OF THE 18 MARCH 2007

LAHAR AT MT. RUAPEHU, NEW ZEALAND

A THESIS SUBMITTED TO THE GRADUATE DIVISION OF THE
UNIVERSITY OF HAWAI'I AT MĀNOA IN PARTIAL FULFILLMENT
OF THE REQUIREMENTS FOR THE DEGREE OF

MASTER'S OF SCIENCE

IN

GEOLOGY AND GEOPHYSICS

DECEMBER 2010

By

Brian C. Kastl

Thesis Committee:

Sarah Fagents, Chairperson
Bruce Houghton
Scott Rowland

Keywords: lahar, deposition, grain size distribution, stratification, basal flow

ACKNOWLEDGEMENTS

ABSTRACT

Spatiotemporal variability in the deposits of lahars offers insights into the characteristics and fluid dynamics of these sediment-laden flows. The 18 March 2007 Crater Lake break-out lahar at Mount Ruapehu, New Zealand, emplaced 1.4 million m^3 of both massive and bedded deposits over the first 47.4 km of its flow path. Traditionally these would be classified as debris flow and hyperconcentrated flow deposits, respectively. Grain size and componentry analyses were performed on samples collected over the first 11 km of the flow path, for both the 2007 lahar itself and pre-existing deposits that contributed sediment to the lahar. Altered landslide material contributed a major proportion of sediment to the flow 400–800 m from the source of the lahar, and was used as a marker to understand downstream evolution of flow characteristics. Variations in the proportions of this altered landslide material with grain size and distance suggest that abrasion and cataclasis occurred during transport. Furthermore, altered landslide clasts are more rounded than all other sediment types, demonstrating greater susceptibility of the former to mechanical breakdown, which influences flow rheology. Ten of sixteen samples of the 2007 lahar deposit exhibit bimodal grainsize distributions. Primary modes coarsen with depth at locations where samples could be collected at multiple depths, while distinctive weak sand-sized (1–2Φ) secondary modes become more pronounced with depth in the deposit. Sand-sized primary modes exist 7 km from source, in deposits near the head of a side channel that captured the upper portion of the lahar after it overtopped a drainage divide.

We put forth a model for deposition in the first 11 km reach by the waning phase of a lahar with a concentrated basal flow and a strong vertical sediment concentration gradient. As the sediment concentration of the flow reached its peak, the basal region generated sand grains through abrasion and cataclasis during intergranular collisions. This sand was also transported in the upper dilute transport region of the current and is preserved as secondary modes in deposits produced by rapid vertical accretion. As the sediment concentration of the flow decreased over time, turbulence increased in the basal flow, causing selective, incremental deposition of sediment now depleted in sand, and ultimately finer-grained, stratified deposits. Our results support the concept that deposit

characteristics are highly dependent on the stratification of the flow and the depositional regime, both of which evolve over time and are controlled by the sediment concentration and flow competence.

TABLE OF CONTENTS

LIST OF TABLES

LIST OF FIGURES

CHAPTER 1. INTRODUCTION

1.1 Geologic Setting

Mount Ruapehu rises to 2797 m above sea level on North Island, New Zealand (Fig. 1) and is the largest and most active andesitic composite cone of the Taupo Volcanic Zone (Hackett and Houghton, 1989). The Whangaehu Gorge represents the most proximal section of the Whangaehu River, dissecting the eastern flank of the edifice from the summit to a distance of 10 km. The gorge has experienced one of the highest lahar frequencies in the world, with over 50 recorded since 1861 (Graettinger 2010). It has been the dominant lahar path over the last c. 2 ka, and a comprehensive sedimentary record is preserved in the Whangaehu Fan, located 10–23 km from the summit (Lecointre et al., 2004; Hodgson et al., 2007). Here Holocene fluvial and phreatomagmatic tephra deposits indicate that the summit Crater Lake has existed for c. 2000 years (Cronin et al., 1997; Cronin and Neall 1997; Donoghue et al., 1997). Lying at an elevation of 2530 m, the lake contains 7–11 million m^3 of warm, acidic water (Christenson and Wood 1993).

Lahars at Ruapehu have a variety of triggering mechanisms, including ejection of Crater Lake water during eruptions, remobilization of unconsolidated tephra deposits by heavy rainfall, flank collapses, and Crater Lake break-out floods (Cronin et al., 1996, 1997b; Manville et al., 2000; Lube et al., 2009; Kastl and Manville, in review). For example, expulsion of Crater Lake water by eruptive activity produced snow-slurry lahars and dilute lahars during both the 1995-1996 eruption sequence and the September 2007 hydrothermal explosion, which occurred after the lahar of this study. Snow, ice, and sediment from the summit and valley glaciers, streambed, and former lahar terraces were incorporated into the lahars during these events (Cronin et al., 1996, 1997b; Lube et al., 2009). Intense periods of rainfall also readily remobilized fall deposits from the 1995-1996 eruptions (Cronin et al., 1997b; Hodgson and Manville, 1999). A shallow slope failure 4.6 ka ago quickly mobilized into a lahar, leaving thick deposits in the Whangaehu Gorge (Kastl and Manville, in review). Prior to the 18 March 2007 lahar of this study, the most recent Crater Lake break-out lahar at Ruapehu occurred on 24 December 1953 when a barrier of unconsolidated tephra from the 1945 eruption sequence failed, releasing approximately 1.8 million m^3 of water into the upper gorge (Manville, 2004). This lahar

destroyed a railway bridge 39 km from Crater Lake, resulting in 151 fatalities when a train plunged into the river bed (O'Shea, 1954).

Eruptions in September-October 1995 and June 1996 deposited 7-8 m of tephra at the outlet from Crater Lake, which formerly drained over a competent rock rim into the Whangaehu Gorge (Manville et al., 2000; Manville, 2004; Manville and Cronin, 2007). As the lake level rose above the rock rim in January 2006, the water was confined initially by the weak, unconsolidated tephra deposit (Massey et al., 2009). A lake break-out lahar as a result of failure of the tephra dam was forecast (Hancox et al., 2001), and the impending flow was predicted to bulk rapidly by entrainment of sediment, including 3–7.5 million m^3 of moraine, talus, slide debris, and alluvium available in the Whangaehu Gorge downstream from Crater Lake (Hancox, 2002). This event took place on 18 March 2007 and is the focus of this thesis.

1.2 Purpose of The Study

The dynamics of lahars are complex and profoundly influenced by changes in sediment concentration. The addition and loss of sediment and/or water to the lahar during transit controls quantities such as volume, flow depth, and velocity (Pierson and Scott, 1985; Vallance, 2000; Manville, 2004). Severe challenges therefore exist for predicting runout, inundation area, and travel times because models of lahar emplacement commonly fail to incorporate the roles of bulking or debulking of the moving current (Iverson and Vallance, 2001; Iverson, 2005; Carrivick et al., 2009).

The aim of this study is to develop an improved understanding of the temporal and spatial evolution of the 18 March 2007 lahar through comprehensive analysis of deposit samples, coupled with field investigations of inundation heights and data collected during the event by a suite of instruments deployed along the flow path. This study focuses on the upper 11 km of the flow path, which saw the most pronounced changes in flow dynamics and lahar properties (Manville et al., in review). Over this reach we acquired 30 samples of the March 2007 deposit, as well as the sediment sources

available for erosion by the lahar. We subjected these samples to field and laboratory analyses including grain size distribution, lithologic componentry, and component angularity. The analyses yield insights into the transport processes and characteristics of the March 2007 Ruapehu lahar.

CHAPTER 2. BACKGROUND

2.1 Characteristics of lahars

2.1.1 Classification of sediment-laden flows

Composite volcanoes are particularly prone to hazardous sediment-laden flows due to their steep slopes and abundance of unconsolidated sediment (Manville et al., 2000; Vallance, 2000). Inhabitants and infrastructure in downstream river valleys are vulnerable to the unpredictable changes in the behavior of flows, which commonly increase in volume with distance (Pierson and Scott, 1985). Lahars are primarily classified according to solids content, which influences both flow behavior and deposit characteristics. However, direct measurements of solids content are challenging (Cronin et al., 1999; Manville et al., 2000) and observations of active flows and the resulting deposits provide only limited understanding of internal flow dynamics. Consistencies between classification schemes and measured or observed phenomena are thus difficult to establish. Spatiotemporal variability in sediment concentrations during an event introduces additional problems with traditional one-dimensional classification schemes that do not consider concentration heterogeneity over time, with depth in the flow or laterally across the lahar channel.

Lahars typically encompass a range of sediment concentrations, from ~20–80% by volume. At the dilute end of the spectrum, hyperconcentrated streamflows are defined as containing 20–60% solids by volume (40–80% by weight; Beverage and Culbertson, 1964). Observations indicate that their flow surfaces are muddy, yet watery, with few visible clasts (Pierson, 2005b). The transition to measurable yield strength denotes the lower threshold of the hyperconcentrated flow classification (Pierson and Costa, 1987).

Debris flows contain 60–80% solids by volume (80–90% by weight) and demonstrate significantly different flow dynamics and deposit characteristics due to increased grain-to-grain interactions (Costa, 1988). The higher sediment concentrations dampen turbulence and reduce the role of water as the transporting medium. Instead, a suspension of water, silt, and clay particles provides pore fluid pressure, thereby facilitating motion by reducing intergranular friction between clasts (Iverson, 1997).

Sizeable boulders may be visible on the surface and margins of debris flows (Pierson, 1986).

Deposit characteristics are also related to sediment concentrations. The depositional features of hyperconcentrated flows cannot be fully attributed to turbulence as they are for dilute flood deposits because increased sediment concentration dampens turbulence and gravitational settling may play a more significant role (Smith, 1986; Costa, 1988). Hyperconcentrated flow deposits are typically poorly sorted and bedding exhibits horizontal or cross-stratification and occasional imbrication (Smith, 1986). Deposition may be rapid, but is nevertheless incremental, not *en masse* (Smith, 1986). Debris flows, having greater yield strengths, may experience *en masse* deposition when intergranular friction reaches a threshold, causing the flow to lock up and cease motion (Iverson, 1997). However, incremental accumulation commonly occurs if intergranular friction remains low (Major, 1997). Regardless of depositional style, debris flow deposits are typically matrix-supported, very poorly sorted, seldom show bedding, and may be inversely graded (Vallance, 2000).

Lahars are also classified according to the amount of clay within the flow, independently of classification by total sediment content. "Cohesive flows" have 3–5 % by volume clay, whereas "non-cohesive" flows have <3% clay. Cohesive flows maintain their sediment concentrations over great distances (Scott et al., 1995), leading to greater run-out distances, and thus pose enhanced threats to surrounding infrastructure and settlements (Vallance and Scott, 1997).

2.1.2 Downstream flow transformations

Transformations between flow types can occur repeatedly with distance and time, due to bulking (erosion and assimilation of external sediment), debulking (loss of sediment), dilution (addition of water, for example, from tributary inflows or melting of assimilated snow or ice), and less significantly, infiltration processes (loss of water to the channel bed; Pierson, 1985; Fagents and Baloga, 2006). Transformations between dilute floods, hyperconcentrated stream flows, and debris flows may be bidirectional (Pierson 1985;

Manville et al., in review). For example, a hyperconcentrated flow may evolve into a debris flow through entrainment of sediment and then later evolve back to a hyperconcentrated flow. A rapid transformation from a solids-dominated slope failure to a more dilute, highly mobile debris flow may also occur within a few kilometers of the collapse (e.g. Vallance and Scott, 1997; Kastl and Manville, in review).

The ability of flows to transform is influenced by clay content (Vallance and Scott, 1997), which in turn may be related to source characteristics. Non-cohesive flows commonly exhibit transformations due to sediment loss, whereas cohesive flows lose sediment less readily (Scott et al., 1995).

2.1.3 Spatial and temporal variability

Lahars with low to moderate solids concentrations commonly exhibit a range of characteristics along their longitudinal axes, which may be broadly divided into head, body, and tail regions (Fig. 2a; e.g., Vallance, 1994; Cronin et al., 1999; Manville et al., 2000). The head of the lahar is the most dilute and erosive, and is associated with the rising limb of associated hydrographs. Considerable debate exists about the reason for the low sediment concentration of the head (Cronin et al., 1999; Manville et al., 2000). It has been observed to consist of a dilute upper layer underlain by a sediment-rich basal layer (Cronin et al., 1997b). Sampling of active flows down to 1 m suggests that dilute fluid may be pushed forward by the underlying denser, sediment-laden flow (Cronin et al., 1999). Alternatively, the concentrated pulse may propagate beneath the existing stream water (Manville et al., 2000).

The head is followed by a mixing zone, where sediment concentrations progressively increase towards those of the main body. The mixing zone progressively lengthens as a function of distance from source (Figs. 2a and 2b; Vallance, 1994). The body of the lahar contains the highest sediment concentration, largest median grain size, and greatest sediment discharge, although the peak sediment concentration may lag behind peak discharge (Fig. 2a; Vallance, 2000).

6

The tail is associated with the falling limb of the hydrograph (Hodgson and Manville, 1999; Vallance, 2000), gradually waning in discharge and sediment concentration, as the flow declines over time in its competence to transport large clasts (Figs. 2c and 2d; Vallance, 1994; Cronin et al., 1999; Manville et al., 2000). Decreasing flow competence with time may result in increasing grain sizes with depth in the deposit (Vallance, 1994).

In addition to this variability throughout both the length and duration of the lahar, the potential for surges and instabilities to develop in the flow has significant implications for the timing of erosion and deposition as well as for deposit bedding, grading, and grainsize characteristics.

2.1.4 Stratification and turbulence in lahars

Dip-sampling and deposit studies of hyperconcentrated lahars suggest that vertical gradients in sediment concentration and velocity exist, such that the base maintains the highest solids content and lowest velocities (Hanes and Bowen, 1985; Bradley, 1986; Sohn, 1997; Cronin et al., 1997b; Manville and White, 2003; Pierson, 2005; Ghoshal and Mazumder, 2005). Direct dip techniques have, however, only sampled the surfaces of flows, rarely penetrating >1 m in depth (e.g. Pierson and Scott, 1985; Arboleda and Martinez, 1996; Cronin et al., 1997b). Gradients in solids concentration and grain size appear to be more nonlinear towards the base of the flow due to gravitational settling (Manville and White, 2003). A basal layer thus develops, with characteristics and behavior of an overall denser flow (Fisher, 1983), overridden by the more dilute portion of the flow carrying predominantly fine material only (Pierson and Scott, 1985). Experimental studies also predict this stratified flow regime (Fahnestock and Haushild, 1962; Cheel and Middleton, 1986; Larcher et al., 2007).

Hyperconcentrated lahar deposits may be more representative of the basal part of the flow than of the entire flow itself (Pierson and Scott, 1985; Manville and White, 2003). Higher particle concentrations within the basal layer are responsible for lower turbulence than in the upper dilute portion of the flow (Smith, 1986; Costa, 1988),

allowing gravitational deposition of primarily the lowermost sediment (Manville and White, 2003). At greater overall sediment concentrations, turbulence is dampened throughout the entire vertical extent of the flow, and particle settling is consequently hindered (Ghoshal and Mazumder, 2005). Once sediment concentrations reach 40% by volume, the mid-range for a hyperconcentrated flow, the downward movement of particles is dominated by percolation through voids between clasts as the flow shears and vibrates, rather than by gravitational settling (Beverage and Culbertson, 1964; Vallance, 2000). Large particles move upwards through squeeze expulsion, ultimately leading to inverse grading in active flows with high sediment concentrations (i.e., debris flows; Vallance 2000) in a process known as kinetic sieving.

2.1.5 Bulking and erosional regimes

Entrainment of sediment into a lahar (i.e., bulking) has a significant impact on volume, advance rate, density, and ultimately hazard potential (Fagents and Baloga, 2006). Ample volumes of sediment for lahar bulking are generated on composite cones, and volcaniclastic deposits are readily available for entrainment by the lahar (Manville et al., 2000). The early, dilute phase of lahar flow (Fig. 2) experiences the most rapid entrainment of external sediment (Cronin et al., 1999; Rodolfo et al., 1996). During this time, the streambed may be eroded to a lower level (Cronin et al., 1999) only shortly before the lahar may begin deposition at the same location, making deposit thickness calculations challenging, even with accurate pre- and post-lahar elevation data (cf. Manville et al., in review).

As the limit of capacity (the maximum volume of sediment a flow can hold) is approached, lahars lose their ability to entrain additional material from the stream bed (Hiscott, 1994), after which lateral erosion, including bank collapses, contributes proportionally greater volumes of sediment to the flow (Rodolfo et al., 1996). For lahars produced by water released from a crater lake, the ratio of peak lahar discharge (at any given distance downstream) to peak water discharge from the crater lake can be used to calculate bulking factors, which provide a proxy for the capacity of the lahar (e.g. Scott,

1988; Vallance and Scott, 1997; Scott et al., 2005; Manville, 2004). Bulking factors (unitless) indicate the increase in flow volume with time and distance, as a result of the entrainment of external material. Bulking factors are influenced by the geometry of the flowpath and nature of available sediment (Pierson, 1995; Manville et al., in review), and by peak discharge (Cronin et al., 1997b). Bulking factors of historic lahars in the Whangaehu Gorge range from 3 to 5.7 (Manville, 2004).

2.1.6 Debulking and depositional regimes

The depositional regime and thickness of the basal portion of stratified flows significantly influences deposit properties. Incremental deposition of the coarsest clasts (Vallance, 1994) from the lowest portion of the basal flow commonly occurs as the basal flow decelerates and the competence of the lahar decreases (Baker and Ritter, 1975; Costa, 1983; O'Conner, 1993). During rapid incremental deposition, clusters of clasts or longitudinal bars are deposited (Vallance, 1994). In these cases the deposits are not snapshots of the flows. However, when the pore pressure of the basal flow is significantly reduced, a more continuous basal deposit is emplaced (Major, 2000), with grain size and sorting characteristics that more closely resemble those of the active basal flow.

Massive, poorly sorted deposits have been produced in high sediment concentration flume experiments by progressive vertical accretion, emphasizing that flow properties cannot necessarily be interpreted from deposit characteristics, and suggesting that *en masse* deposition may occur under unique conditions (Major, 1997; Major and Iverson, 1999). Such experimental flows have maintained substantial pore fluid pressures between flow deceleration and deposition, preventing *en masse* deposition (Major and Iverson, 1999). Deposition of the full flow thickness could, however, occur if low pore fluid pressure allows rapid deposition of coarse material at flow margins, causing unusually rapid deceleration and acting to dam upstream material (Major and Iverson, 1999).

The potential to preserve stratigraphic records of temporal variability in depositional regimes is low unless the solids concentration significantly changes; even units from distinct flow pulses are often indistinguishable within deposits (Weirich, 1989; Hodgson and Manville, 1999). Remnant pore fluid pressure slows consolidation, allowing subsequent flows to degrade contacts between events (Major and Iverson, 1999).

2.1.7 Abrasion and cataclasis

Both cohesive and non-cohesive lahars have demonstrated progressive downstream cataclasis (clast fracturing) and abrasion (clast rounding) (Scott, 1988; Vallance and Scott, 1997).   These processes may significantly reduce both the size of individual grains and the grain size distribution of the sediment load, particularly during rapid flow (Schumm and Stevens, 1973). Experimental studies indicate that rounding of volcanic clasts takes place much more rapidly (over transportation distances up to an order of magnitude less) than for non-volcanic material (Pearce, 1971), probably because the volcanic clasts are more likely to be weathered or altered (Bradley, 1970; Kodama, 1994). Futhermore, the vesicular nature of many volcanic clasts may increase abrasion rates. Cataclasis and abrasion of poorly sorted sediment may take place with little downstream movement if grains are subjected to particularly strong lift and drag forces (during, for example, high-discharge events), but are obstructed by other particles and prevented from further downstream motion (Schumm and Stevens, 1973).

2.1.8 Grain size bimodality

Grain size histograms of the deposits of sediment-laden flows may exhibit bimodality, with a primary mode at a large grain size, and a significantly smaller secondary mode at a smaller grain size (Vallance and Scott, 1997; Vallance, 2000; Manville and White, 2003; Rădoane et al., 2008). Sand-sized secondary modes commonly increase in magnitude as a function of transport distance for coarse-grained lahar and non-lahar river settings in which abrasion and cataclasis have been shown to play a role in downstream fining

(Kodama, 1994; Vallance and Scott, 1997). As the abundance and size of boulders decrease with distance, a deficiency centered at -1Φ develops and a secondary mode centered at 2Φ increases in magnitude (Kodama, 1994; Vallance and Scott, 1997). Manville and White (2003) explain that bimodality in a stratified flow regime may be caused by the simultaneous deposition of boulders and sand, allowing fine-grained matrix sedimentation (including sand) as flow capacity is lost, and boulder emplacement as flow competence is reduced. Alternatively, Rădoane et al. (2008) suggest that similar secondary modes are caused by sediment contributions from tributary streams, although a progressive increase in the secondary mode intensity is observed in their data with distance, instead of step-wise increases as might be expected immediately downstream of stream confluences.

2.2 The 18 March 2007 Crater Lake Breakout lahar

Following the 1995-1996 eruption sequence at Mount Ruapehu, Crater Lake (Fig. 3b) re-filled at irregular rates (Manville and Cronin, 2007), rising above the level of the rock rim and becoming impounded by the 1995-1996 tephra deposit in January 2006. Seepage and localized erosion through the south side of the tephra barrier were identified between 24 December 2006 and 5 January 2007 (Massey et al., 2009). The lake level rose 30 cm during a period of wet weather from 13–15 March 2007 (Massey et al., 2009), reaching its highest level c. 6.4 m above the solid rock rim on the morning of 18 March 2007 during another period of intense rainfall (Carrivick et al., 2009). Accelerated erosion and slumping ensued, and at 11:22 (NZST) the tephra dam failed (Fig. 3b), releasing 1 million m^3 of water into the Whangaehu Gorge over 90 minutes (Manville and Cronin, 2007; Massey et al., 2009; Manville et al., in review). Peak discharge from Crater Lake was calculated at 548 m^3/s (Manville et al., in review). At 6 km from source the average solids concentration reached a maximum of 51% by volume, averaged over the duration of the event, having entrained snow ice, and sediment (Manville et al., in review).

The terrain encountered by the lahar in the gorge was highly variable, including chute-and-pool sequences in the upper gorge, occasional bedrock confinement, abrupt channel narrowing and widening, and three bifurcation locations. A landslide 400–800 m from source was re-activated when the toe of an old landslide deposit was undercut (Fig. 3c). The new landslide dammed the flow and was breached several times to contribute 846,300 m^3, or 29% of upper gorge sediment, to the lahar (Massey et al., 2009; Manville et al., in review). A peak flow of 2500 m^3/s was derived from a radar stage gauge located at 7 km downstream of the Crater Lake outlet (Fig. 3d) (Manville et al., in review). The lahar emerged from gorge confinement and reached the apex of the alluvial fan, 10 km from source, after ~30 min (Carrivick et al., 2009). The lahar reached the alluvial fan (Figs. 1 and 3e), splitting into a braided system and leaving alternating tracts of net deposition and erosion (Manville et al., in review). Upon reaching the Rangipo Fault scarp at 17.4 km from its source, the lahar's distributaries coalesced (Graettinger et al., 2010) to follow the Whangaehu River Valley. Erosion outweighed deposition by a factor of three over the first 47.4 km of the flow path, where 4.5 million m^3 of material was eroded, 65% of which was sourced from the upper gorge, and 1.4 million m^3 was deposited (Manville et al., in review). The lahar ultimately entered the Tasman Sea, 215 km away, 17 hours after onset (Massey et al., 2009).

2.3 Previous work on the deposit

An unprecedented array of real-time data were collected in the Whangaehu Gorge, fan, and River to study emplacement processes of the 18 March 2007 lahar. Data collection was carried out using radar stage gauges, geophones, a broadband seismometer, and digital video (Manville and Cronin, 2007). A time-lapse camera recorded headwall retreat of erosional scarps in the tephra dam before geophones and a telemetered tripwire detected passage of the lahar (Massey et al., 2009).

Pre- and post-event channel cross sections and post-event "high water marks" were traced using a differential Global Positioning System (dGPS; S. Fagents unpublished data). Additional field observations of high water marks suggest that they

formed during short-term increases in stage height, discharge, and bulking (Graettinger 2007) and that they correlate positively with the degree of channel confinement (Manville et al., in review).

Joyce et al. (2009) contrasted the accuracy of various satellite and airborne remote sensing techniques for deriving the path of the lahar and found that SPOT5 (Satellite Pour l'Observation de la Terre) was individually most reliable, although a combination of satellite and light detection and ranging (LiDAR) topography was more accurate, identifying up to 92% of the lahar's inundation area. High resolution orthophotographs were used as a reference for accuracy.

Carrivick et al. (2009) compared real-time data to velocity predictions generated by Delft3D, a fluid dynamics model, and discovered some agreement with gauged flow deceleration over the Whangaehu Fan and acceleration along the Whangaehu River. Modeled flow front velocities have the greatest discrepancies with real-time data due to effects such as surface roughness and topographic variability along the flow path. Carrivick et al. (2010) recognized that temporal variability in sediment transport processes heavily impact modeling accuracy. They therefore integrated a series of real-time hydrological measurements with volumetric analysis of erosion/deposition from LiDAR surveys (cf. Manville et al., in review) and found that 75% of erosion occurred during the period 10–40 minutes after the breakout.

Manville et al. (in review) compared pre- and post-lahar LiDAR topographic survey data to derive topographic changes, erosional and depositional volumes, and sediment concentration models throughout the gorge and valley. This study determined that 65% of erosion occurred in the upper gorge, including 8.4×10^5 m^3 from the syn-lahar landslide, with negligible deposition in the first 4.5 km of the flow path. Mass balance models suggest that the lahar's capacity limit was reached approximately 6 km from source where the bulk sediment concentration reached 51% by volume. Maximum deposition occurred between 6 and 7 km from source. Erosion to depths of 2–4 m took place in a 400 m long side channel (Fig. 3d), which the lahar reached by overtopping a drainage divide 7 km from Crater Lake, while the bulk of the flow continued in the main channel. The propensity for erosion in the side channel suggests either a dilute peak

13

discharge or a vertically stratified flow (Manville et al., in review). The minimum bulk sediment concentration in our study area (46% by volume) was achieved 11 km from Crater Lake (Manville et al., in review).

Proctor et al. (2010) analyzed the same topographic survey data and suggested that the high rates of erosion in the upper gorge were due to bank collapses that were easily entrained into the flow due to low sediment concentrations in the dilute upper part of the flow. Proctor et al. (2010) further suggested that spatial variability in erosion and deposition farther downstream on the alluvial fan may be a product of rheological transformations.

With the flow capacity limit reached, variability in flow competence (ability to transport a maximum grain size) therefore exerted the strongest controls on depositional thickness and grain size distributions (Manville et al., in review). Changes in flow velocity, due to variations in channel geometry, had dramatic effects on flow behavior, whereas sediment availability for bulking played a less significant role. Numerous hydraulic and geomorphic parameters were compared with deposit thickness values, but none were systematically correlated. Deposit thickness was most closely correlated (inversely) with the slope of the pre-lahar channel (Manville et al., in review). Grain size distributions, however, did not show a simple relationship with distance from source as would be expected with decreasing competence (Manville et al., in review). This suggests that the lahar had a more complex response to topographic variability, with evolving internal flow dynamics that may be unrecognized and understudied.

CHAPTER 3. METHODS

3.1 Field

Twenty samples of 18 March 2007 lahar deposits and ten samples of potential bulking sediment were obtained in the Whangaehu Gorge 5–11 km from Crater Lake (Figs. 1, 4) over four field campaigns, beginning twelve days after the event and ending on March 27 2009. These include sixteen massive and bedded samples of primary deposits from the main channel and four samples from a side channel in the medial gorge (Table 1). Bulking sediment includes the syn-lahar landslide deposit 400 to 800 m from Crater Lake (Fig. 3c), the 1995 lahar deposits from the main channel, fluvial and alluvial sediment from the side channel (Fig. 3d), and the 1975 lahar deposits from both the main and side channels. Sample locations were based on deposit presence (no 2007 primary deposition occurred <4.9 km from Crater Lake), accessibility, and depth of post-event incision. Insufficient post-lahar incision prevented identification of the 2007 lahar deposit base at any point. For this reason, sample depths relative to entire deposit thickness remain unknown. Deeper samples of all deposits types may be biased towards thicker, more proximal locations because post-event incision generally increases with deposit thickness and decreases with distance from source.

Grain size analysis began by measuring the largest size classes (-8 to -4Φ), which were sieved or measured at 0.5Φ intervals. When exposures were of sufficient size, total sample weights were based on the largest boulder identified at the sample location, such that the boulder's mass represented no more than 5% of the total sample weight. The sieved fractions <-4Φ were coned, quartered and weighed until 0.5–1.0 kg could be retained for later laboratory sieving.

Bedding properties of exposures and the character of the surrounding stream channel were recorded at each sample site. The presence of stratification, grading, clast vs. matrix support, imbrication, visible bimodality, and lenses of clast-supported material were documented, where present. Fine-scale variations in deposit character were recorded in a limited number of detailed stratigraphic logs. Channel attributes

immediately upstream of sample sites, such as abrupt changes in gradient and channel constriction/dilation were noted for later quantification using geospatial analysis.

3.2 Laboratory

3.2.1 Grain size

All $<-4\Phi$ (16 mm) fractions were processed to determine their grain size distribution. Samples were oven-dried at 105°C, reweighed, and water correction factors were applied to the field-sieved weights. Sieving was carried out at 0.5Φ intervals down to 4Φ, using a shaking device for two minutes for each Φ size.

The remaining fines $> 4\Phi$ were analyzed using a Malvern Mastersizer 2000 laser diffraction particle size analyzer after they were reduced in volume using sample splitters, and soaked in sodium hexametaphosphate to prevent aggregation. The instrument produces an observed diffraction pattern and a modeled diffraction pattern, the difference of which is represented by the residual. The standard operation procedure (SOP) for potassium feldspar (refractive index of 1.54 and absorption of 0.1) was chosen because this SOP was tested with 2007 lahar samples against other SOPs and demonstrated the lowest residual. Potassium feldspar additionally has optical properties most similar to the assumed mineral assemblage of fine andesitic grains of this study.   A jagged diffraction pattern was most common for coarser-grained samples, but these samples were reanalyzed until residuals remained below 1.6%. Three twelve-second measurement sets per aliquot were made at a pump speed of 2500 revolutions per minute (RPM) and stirrer speed of 1000 RPM, and averages were calculated to produce volumetric grain size distribution data for all samples.

3.2.2 Componentry

The -3.5 to -2Φ size fractions of the samples were also analyzed to determine the mass proportions of clasts having unaltered vs. altered surfaces. The distinction between altered vs. unaltered clasts was based on a grain-by-grain inspection under the criterion that a grain with red alteration of any thickness, recognizable by the unaided eye, was considered altered. The minimum size limit (-2Φ) of the four analyzed size classes was based on the difficulty of identifying patches of alteration on grains smaller than this size class. Finer grains generally appeared to lack the alteration. The maximum size limit (-3.5Φ) was based on the critical number of grains (nine) needed for sufficient statistically-based accuracy of representation per size class. A binocular microscope was used to identify the crystallinity and mineralogy of 2Φ grain sizes for selected samples. Plagioclase was identified, having similar optical properties to those of feldspar (used as the standard operating procedure for laser diffraction analysis).

3.3 Computational

An overlap of 1Φ and 2Φ class sizes between data produced by the sieving and laser diffraction methods allowed a conversion factor to be calculated in order to combine grain size data into a single histogram for each sample. Adopting a uniform density for all grain sizes, the sieved 1Φ and 2Φ size class weight fractions were divided by the respective laser diffraction volume fractions. The average of these values represents the conversion factor that was applied to all laser diffraction volume fractions to produce final grain size histograms.

In order to test the consistency between the sieving and laser diffraction techniques, and consequently to test the accuracy of combining data from these methods, the margin of error for each conversion factor was also calculated. These values were calculated for all samples by finding the difference between either size class of the converted weight fraction and its respective laser diffraction volume, then dividing by the

converted weight fraction. This method yields the same value for both size classes. Margins of error ranged from 2.1% to 40.9%, with an average of 15.7 % and a standard deviation of 10.7%.

Sample statistics were produced using GRADISTAT Version 6.0 (copyright S. Blott, July 2008), a software program provided in Microsoft Excel format. Grain size data were input and all statistics, such as mean, sorting, skewness, and kurtosis, were calculated using the Method of Moments in Microsoft Visual Basic programming language according to the equations established by Krumbein and Pettijohn (1938).

The geospatial information software program called ArcGIS was used to extract, analyze, and compare all data (i.e. distance from Crater Lake, deposit infilling, and sampling depth associated with samples at their respective locations). Sample locations were recorded using a handheld GPS, transferred to the ArcGIS interface using a freeware program called GPS Utility, and georeferenced to the map grid of aerial photographs and LiDAR-based DEMs. Attributes associated with samples and sample locations, including but not limited to elevations, distances from source, elevation change between pre- and post-event LiDAR topographic surveys, and channel slope, were organized within ArcGIS and later transferred to Microsoft Excel for statistical analyses and graphical representation.

CHAPTER 4. RESULTS

4.1 Field observations

All 30 samples from deposits of this study were collected between 5 and 11 km from Crater Lake, with the exception of the landslide deposit sample, which was collected 600 m from Crater Lake (Fig. 4). These samples can be divided into two main categories: primary deposits of the 18 March 2007 lahar and potential bulking material available to be eroded and assimilated into the active lahar. The former category includes: (i) massive main channel deposits (2007M) with (ii) interbedded clast-supported lenses; (iii) bedded main channel deposits (2007B); and (iv) side channel deposits (2007S), representing the four main units of the 18 March 2007 lahar in the study area. Bulking material includes the 18 March 2007 landslide, the 1975 lahar terraces, 1995 lahar terraces, and miscellaneous side channel alluvial and fluvial material (Table 1).

4.1.1 Primary deposits

The 18 March 2007 lahar was valley confined, and the deposit demonstrated little to no surface relief within the gorge. Massive deposits (2007M) are typically matrix-supported, containing sub-angular to sub-rounded clasts, and comprise the lower portions of deposit exposures, although the basal contacts of primary deposits were not exposed. Clast-supported lenses less than 40 cm in thickness and largely free of fines, are interbedded with, or overlie, massive deposits with similar maximum grain sizes. These lenses are more common at shallower depths (Figs. 5a and 5b). Bedded deposits (2007B) are weakly stratified at the centimeter-decimeter scale, have finer grain sizes than (i) and (ii), and consistently comprise the upper portions of the deposit, overlying 2007M deposits and clast-supported lenses. Deposit surfaces commonly expose the largest boulders in the deposit.

Near the head of the side channel occupied by the lahar 7 km from the lake outlet (Figs. 3d, 6a), isolated deposits 80 cm thick were emplaced adjacent to high relief bedrock and pre-lahar boulders. These deposits are almost entirely matrix-supported with weak bedding and an absence of outsized clasts. In order to reach this side channel, the lahar overtopped a drainage divide at two locations 100 m apart (Fig. 6a). Assuming pre-lahar channel bed elevations during overflow, digital elevation data suggest that the flow exceeded a depth of 3.9 m at the first (upstream) overflow location, and 6.0 m at the second location (A. Graettinger unpublished data). These depths would have led to flow thicknesses entering the side channel of 4.4 m and 2.3 m (47% and 28%, respectively, of peak stage height) during peak flow (Fig. 6b), if the flow thickness at these locations was consistent with those at the radar stage gauge 100 m downstream. According to these assumptions, overflow at the lower (downstream) drainage divide took place for a duration of 1 hour 11 minutes (Fig. 6b). Comparison of the elevations between the pre- and post-lahar DEMs also shows a maximum eroded depth in the side channel of 370 cm, providing an average erosion rate of 5.22 cm/min. However, because erosion and deposition were probably neither constant nor continuous throughout the overflow, instantaneous depositional and erosional rates are likely to exceed these average values.

4.1.2 Material available for bulking

The toe of the syn-lahar landslide was eroded over a distance of 400 to 800 m from Crater Lake by the 2007 lahar, contributing angular, matrix-bearing material to the active flow. Clasts in the landslide deposit show pervasive, yet surficial, yellow-to-red alteration that is typically absent in the interior of clasts (Figs. 5e, 5g). Deposits from the 1995 and 1975 lahars are unconsolidated and had been incised to depths of 3 m by regular streamflow in the gorge prior to the 2007 event, producing a terraced morphology. During the March 2007 lahar, these terraces experienced undercutting and bank collapse to contribute material to the flow. The 1995 and 1975 deposits are commonly matrix-supported, typically more so than the 2007 lahar deposits (Figs. 5d, 5f). At the bases of these terraces, the floors of active and inactive channels were lined with fluvial sediment and lateral bars of unknown depths prior to the event. Within the

side channel, material eroded by the 2007 lahar includes alluvium, fluvial deposits, and 1975 lahar deposits.

4.2 Grain size analyses

4.2.1 Unit descriptions

Grain size distribution characteristics show strong similarities within given deposit classes (Table 2). The 2007M (massive) and 2007B (bedded) deposits contain a dominance of coarse gravel and cobbles, and commonly also show weak, sand-sized weak modes (1–2Φ) that have a more consistent grain size than that of dominant coarse modes (Fig. 7a). While 2007M commonly underlie 2007B deposits, there is no consistent distinction between 2007M and 2007B grain size distribution patterns. The 2007S (side channel) deposits have distinct primary sand-sized modes of similar grain size to the secondary modes of 2007M and 2007B deposits, and they have greater amounts of silt and clay than the other 2007 deposits. Grain size distribution patterns of 1995 and 1975 deposits have primary modes similar to those of the 2007M and 2007B deposits, although secondary modes of fine gravel (-3 to -1Φ) are more common than secondary modes of sand.

4.2.2 Grain size trends with distance and depth

The mean grain size of all lahar deposits ranges from 1.16Φ (medium sand-sized) to -6.92Φ (cobble-sized) (Figs. 8b, 8f). Some grain size trends can be identified with respect to both distance downstream and depth within the deposit. Primary modal grain sizes of 2007M and 2007B deposits range from -4.5Φ to -8.5Φ in the proximal and medial gorge (<8 km from Crater Lake), trending towards -6.5Φ in the distal gorge (>8 km; Fig. 8a). Modal grain size increases with depth for 2007B deposits (Fig. 8e). The 2007B deposits demonstrate the largest and widest range of mean grain sizes, while the only outcrop of 2007S deposits has the finest grain sizes (Fig. 8f). Mean grain size decreases with

distance from Crater Lake for the 1995 and 1975 deposits (Fig. 8b). Sorting of all units is poor to very poor, based on the classification scheme of Folk and Ward (1957), although 2007S deposits are better sorted (Table 2). The 2007M and 2007B deposits have similar ranges of sorting values, and sorting does not improve as a function of distance for either deposit type. Medium sand and clay show the clearest trends out of all class sizes, such that medium sand of 2007M, 1995, and 1975 deposits increases in abundance with distance, while clay content decreases with distance and increases with depth (Figs. 8c, 8d, 8h). Clay fractions are approximately equal for 2007M and 2007B deposits, but 3-4 times greater for 2007S deposits.

Although no modal grain size trends for primary 2007 lahar deposits exist over the entire length of the gorge (Fig. 9), systematic grain size changes are recognized with distance over short reaches, and with depth at single locations. The abundance of medium sand (1-2Φ) generally increases with distance (Fig. 8c). Eight of sixteen 2007M and 2007B samples have weak secondary modes (trough to secondary peak height >0.5% by weight) at either 1Φ or 2Φ, all of which occur >6 km downstream, while three unimodal samples were collected >6 km (Fig. 8). Bimodal 2007 samples acquired <7 km downstream have secondary modes at 1Φ and those >7km downstream have secondary modes at 2Φ (Fig. 9). The weight percentages of the individual Φ class size of the secondary modes range from <1% to 6%. However, there is no consistent variation in the secondary mode weight percentage with distance.

Post-lahar incision into the 2007 main channel lahar deposit was sufficient at three locations to allow sampling at two depth intervals. Grain size distribution patterns of samples from the same site are more similar to each other than are patterns of any two samples from different sites at variable distances downstream (Fig. 7c). In each case deeper samples have notably finer and less distinct primary modes, and similar-sized but stronger secondary modes, than the shallower samples collected at the same location.

4.3 Componentry

4.3.1 Altered clasts

Altered components are found in all 2007 lahar samples. These have rinds of predominantly yellow-to-red material up to 1 mm in thickness. Surfaces of thicker, friable, red material that crumbles to sand and finer grains are also common. These clasts are consistent with the color and texture of altered material in the syn-lahar landslide deposit. Clasts with thinner rinds have surfaces of light orange to a gray similar to the color of the clast interior, particularly along protruding edges (Fig. 10a). Clasts were only classified as altered if red coloration was recognizable. Additionally, rounding and smoothness show an increase with increasing grain size and decreasing degree of alteration (Fig. 10b).

The proportion of altered clasts systematically decreases with decreasing grain size for most 2007 samples. Eight of twelve 2007M samples show progressively lower weight percentages of altered clasts for each 0.5Φ step between -3.5Φ and -2Φ. All 2007B samples show this trend, but the trend is less defined for the smaller size fractions of 2007S samples. Samples of the 2007M and 2007B deposits generally exhibit similar proportions of altered components with averages of 22 and 25% by weight respectively, whereas 2007S samples have an average of only 9% by weight. Although no significant trends exist between the amount of altered components and depth or distance, higher concentrations of altered clasts are largely absent in the distal reaches of the gorge (Figs. 10d and 10e).

4.3.2 Lithologies

The componentry of the 2Φ size class for a 2007S sample and the nearest upstream 2007M sample indicates that qualitatively these two deposits have similar proportions of lithologic components and similar angularity. This 2Φ size class was chosen in order to determine whether the particles of the basal flow (2007M deposits) re-circulate into the transport region (2007S deposits). The lithologies include free crystalline plagioclase, pyroxene, magnetite, hornblende, biotite as well as small fragments of fresh, glassy

23

andesite. The 2007S andesite clasts have marginally higher vesicularities (qualitatively observed), and presumably lower density, than those of the 2007M deposit. Both deposits also contain 2-5% orange-to-red altered particles that are relatively rough and have an appearance closely resembling that of the altered rims of -3.5Φ to -2Φ clasts.

4.4 Key findings

In the main channel of the Whangaehu Gorge, massive, matrix-supported deposits are far more common at depth than bedded, clast-supported deposits. Whereas main channel deposits are boulder-bearing, the side channel deposit is depleted of gravel and larger clasts, and was emplaced after the peak lahar flow partially overtopped a drainage divide. Bimodal samples outnumber unimodal samples in the study area at distances exceeding 6 km from Crater Lake. The grain size of the secondary modes matches that of side channel deposit's primary mode. Older lahar and fluvial deposits that contributed sediment to the flow show no clear imprints on the grain size distribution patterns of the 2007 lahar deposits. However, syn-lahar landslide-derived components can be used as a sediment tracer within downstream lahar deposits and systematically decrease in abundance with fining grain size. They also show increased rounding with distance, compared to unaltered components of the same deposits.

CHAPTER 5. INTERPRETATION

5.1 Bulking and transport

We did not discern traceable signatures of potential bulking material from medial reaches of the gorge (1975 and1995 lahar terraces, alluvium, and fluvial sediment) within the grain size distributions of primary 18 March 2007 samples. For example, the side channel contributed 8,956 m^3 of eroded material (V. Manville, unpublished data) with grain size distribution patterns distinct from those of the 2007 deposits and other contributing sediment types (Table 2). Nevertheless, primary 2007 samples downstream of the re-entry location of the side channel show no obvious enrichment in the most prevalent grain sizes of side channel wall material. We infer that the samples from relatively shallow depths in the 2007 deposits downstream of the side channel were emplaced well after side channel erosion and bulking occurred. This may suggest that the majority of bulking in the gorge took place early in the event prior to the onset of deposition in these locations and/or that deposition of this material took place far downstream from the location of entrainment. The evidence supports the concept that the early erosive, dilute head of a lahar (Fig. 2) can entrain external sediment rapidly (Vallance, 1994; Rodolfo et al., 1996; Cronin et al., 1999; Manville et al., 2000), and in this instance was responsible for the highest bulking rates along the Whangaehu Gorge.

The side channel is a unique location that experienced net erosion with only localized deposition. This 500 m long drainage experienced only a portion of the peak discharge of the dilute upper portion of the flow (Fig. 6). Erosional depth estimates are difficult to constrain throughout the remainder of the lahar flow path because most erosional surfaces are overlain by deposits of uncertain thicknesses, providing only net values of erosion and deposition (cf. Manville et al., in review). A well constrained maximum erosional depth and duration within the side channel, however, allows calculation of an average erosion rate of 5.22 cm/min, but this was probably exceeded during peak stage height when the side channel flow depth was at its greatest. The eroded side channel bulking material (Table 2) was better sorted and finer grained than the main channel sediment, and this may have allowed for higher rates of erosion. High erodability in the side channel is also related to the fact that the overflow event at its

upstream drainage divide allowed only the upper, more dilute part of the mobile flow to be transported through this reach (see section 5.3).

Whereas early erosional stages of lahars commonly entrain high proportions of streambed material, the later stages of erosion are dominated by bank collapse contributions, caused by undercutting (Rodolfo et al., 1996). The only primary 2007 deposit samples that we were able to access in the Whangaehu Gorge are from relatively shallow depths (Table 1) and were thus probably emplaced during the waning stage of the event. Any locally contributed material within these samples would therefore have been derived from intermittent bank collapses of 1975 and 1995 lahar terraces (Figs. 5d, 5f), somewhere upstream of each sample location. Approximately 90% of the 2007 lahar path in the study area 5–11 km from source is lined by these terraces, with heights of up to 8 m above the pre-lahar streambed. In fact, pre- vs. post-lahar LiDAR topographic analysis shows that numerous bank collapses occurred throughout the study area (Manville et al., in review). However, 2007M (massive) and 2007B (bedded) deposits show no characteristic grain size signatures from 1975 and 1995 lahar terraces. Terrace samples typically have primary modes between -7Φ and -8Φ and are poor in sand, whereas 2007 lahar samples more commonly have primary modes at -6Φ, and have minor secondary modes between 1Φ and 2Φ (Table 2). Little downstream grain size variability among 2007 samples (Fig. 9) and even less grain size variability with depth (Fig. 7c), suggests that there are also no spikes in terrace contributions, in either space or time, for the later stages of the lahar recorded by our samples. Thus terrace grain sizes do not overprint 2007 lahar grain size distribution patterns. Instead, the later stages of the 2007 lahar appear to maintain consistent grain size distributions that may be more representative of conditions of internal flow dynamics, including thorough mixing and long distance sediment transport. The presence of altered clasts in shallow deposits suggests that the syn-lahar landslide was actively contributing material for the duration of the event.

The maximum time-averaged sediment concentration peaked at 51% by volume only 5 km from source (Manville et al., in review) due to high sediment availability in the proximal gorge (Hancox, 2002). The location of peak sediment concentration

corresponded to the onset of net deposition in the gorge and the 2007 lahar continued to debulk downstream with a gradual decrease in sediment concentration (Manville et al., in review). Enhanced debulking associated with declining sediment concentration occurred at 5 km because the flow's capacity to hold material decreased (Manville and White, 2003), probably as a response to channel slope shallowing and channel widening. With a diminishing ability to carry material and a predominent debulking regime during the waning phase of flow, entrainment of fresh material would have been minimal, which is in agreement with the absence of traceable terrace grain size signatures in the 2007 samples.

5.2 Debulking

The absence of distinct downstream trends in the grain size statistics of 2007M (massive) samples indicates that a general downstream decrease in flow competence, which would be expected during waning total discharge (Fig. 6b), was not the primary control on grain size. Channel gradient is known to have a first-order control on flow competence, which is related to peak shear boundary stress or unit stream power (Baker and Ritter, 1975; Costa, 1983; O'Conner, 1993). This is also the case for the 18 March 2007 lahar (Manville et al., in review). In other streams, strong positive correlations exist between particle size and mean shear stress for bedload transported during high energy flood events (Baker and Ritter, 1975). However, mean and modal 2007M grain sizes in the gorge do not decrease with distance in the Whangaehu Gorge (Figs. 8a, 8b) even though channel slopes decrease between 5 and 11 km from Crater Lake. The average slope decreases by 35% from the three most upstream samples at 4.7 km from Crater Lake (average 0.064 m/m) to the downstream-most samples at 11.1 km (average 0.048 m/m) (V. Manville, unpublished data). However, the mean and modal grain sizes of these downstream samples are generally greater than the average of those throughout the gorge, despite the shallow depth of sampling in this downstream region (Figs. 8a, 8b). Linear regression analyses between grain size statistics and the channel properties, such as slope and hydraulic radius, which constitute stream power and shear boundary stress equations,

show no significant correlations. Such correlations typically exist for competence-limited flows (cf. Baker and Ritter, 1975; Costa, 1983). These results therefore indicate that flow competence was not the primary control on deposition during emplacement of 2007M deposits.

Grain size distributions of the 2007 Whangaehu lahar are most dependent on depositional style. The lahar had a 47-51% by volume average sediment concentration over the duration of the event in the study area (Manville et al., in review). With the peak bulking factor of 3.4 reached 5 km from Crater Lake, debulking over the next 7 km of our study area was a response to a capacity limit (Manville et al., in review), instead of a competence limitation. It is common for sediment-laden flows to lose entrainment and transport abilities when sediment concentrations are highest and capacity is reached (cf. Hiscott, 1994), particularly in relatively proximal locations (Fig. 2a) such as in our study area.

It is generally assumed that shortly after the passage of a lahar head in the proximal reaches, peak total discharge is reached and followed by peak sediment concentration, both of which wane for the remainder of the event (Fig. 2a; Vallance, 2000). Samples from earlier phases of the flow, namely the 2007M massive deposits, are therefore associated with a higher capacity limitation and a low competence limitation. The shifts to clast-supported deposits and 2007B bedded deposits mark transitions to deposition caused by competence limits (Fig. 11).

The sample data represent an uncertain phase of the lahar due to an absence of accurate deposit thicknesses. Post-lahar incision had not exposed the base of the deposit at any of our sample locations and total deposit thickness data are therefore unavailable. LiDAR-based elevation changes represent only minimum deposit thicknesses (Table 1) because the elevation changes represent the combined effects of erosion and deposition. Samples 38-08 and 38-09, for example, were collected from depths up to 400 cm, but the deposit thickness may well exceed the net elevation increase of 581 cm suggested by LiDAR data (Manville et al., in review).

5.2.1 Massive deposits (2007M)

Under the conditions of capacity-limited flow, the 2007M deposits were probably emplaced through rapid vertical accretion as grain-to-grain friction and bed contact with unsorted basal flow induced deposition (cf. Major, 1997). Facies analysis of lahars at Mount St. Helens also associated matrix-supported deposits, closely resembling 2007M deposits, with peak flow (Scott, 1988) and the thickest deposits of lahar sequences (Walton and Palmer, 1988). Although positive correlations may exist between deposit thickness and grain size (Walter and Palmer, 1988), grain sizes of 2007M samples in the Whangaehu Gorge are not significantly different from thinner 2007B deposits. The absence of sorting and grain size trends with depth in the 2007M deposits indicates that preferential particle size deposition did not occur. The 2007M grain size statistics therefore do not provide an indication of flow competence, probably because deposition occurred rapidly during a period of high sediment concentration, leading to high intergranular forces, and perhaps resulting in frictional locking of the lower portion of the flow. Although the 2007M deposits do not demonstrate mean grain size trends with distance, similarly unsorted and matrix-supported 1975 and 1995 deposits decrease in grain size with distance. This suggests that flow competence may have exerted a weaker control on depositional style during the 2007 lahar, perhaps because rapid bulking of proximal landslide material caused a capacity limitation to be reached.

5.2.2 Clast-supported lenses

Spatiotemporal variability in the characteristics of the 2007 deposits may be due to changing depositional styles associated with decreasing sediment concentrations caused by rapid debulking in the proximal reaches of the study area (<5 km) during emplacement, and a transition from a capacity-limited flow regime to a competence-limited flow regime (Fig. 11). Clast-supported lenses within 2007M deposits (Figs. 5a, 5b) have far better sorting than the rest of 2007M deposits, indicating that the coarse fraction locally settled on the channel bed independently of finer material that remained

in transport. Flow competence probably controlled the clast size distributions in the lenses. Longitudinal bars or clusters of clasts are known to form during incremental deposition through selective emplacement of the coarsest clasts when flow competence becomes insufficient for continued transport of those size fractions (Baker and Ritter, 1975; Vallance, 1997). Clast-supported facies similar to Whangaehu clast-supported deposits exist as basal-flow whaleback bars at Mount St. Helens (Scott, 1988). Furthermore, like the clast-supported deposits in the Whangaehu Gorge, this facies constitutes only approximately 1% of Mount St. Helens deposits and Oligocene-Miocene lahar analogs (Scott, 1988; Walton and Palmer, 1988). In the Whangaehu Gorge, these unique clast-supported units in the 2007 deposits are primarily found at shallower depths, corresponding to passage of the lahar's late body to early tail (Fig. 2) and after earlier debulking had lowered sediment concentrations (cf. Vallance, 1994; Cronin et al., 1999; Manville et al., 2000). Flow surges or instabilities, seen in the jagged nature of the flow depth data (Fig. 6b), may have induced temporal variability in sediment concentration and consequently could have caused such clast-supported lenses to form within 2007M deposits.

5.2.3 Bedded deposits (2007B)

Bedded 2007B deposits demonstrate a late-stage, competence-limited, turbulence-influenced depositional style. Overlying both 2007M deposits and clast-supported lenses, the 2007B deposits were emplaced during passage of the lahar tail (Fig. 2), as sediment concentrations and discharge waned to the point that flow competence was insufficient to transport the largest clasts (Cronin et al., 1999; Manville et al., 2000). Whereas grain size distributions of 2007M deposits show no relationship with inferred flow competence, 2007B deposits increase in modal grain size with increasing depth (Fig. 8e). Lahar volumes in the Whangaehu Gorge, modeled as a function of distance, confirm that the lowest average flux and lowest average sediment concentration in our study area occurred in the most downstream location (Manville et al., in review). The dilute, late stage of lahar passage probably produced the bedded sedimentary features (Figs. 5a, 5b) through

turbulence, as commonly occurs with a reduction in sediment concentration (cf. Fisher, 1971).

5.2.4 Tracing debulking

The landslide, 400 to 800 m from Crater Lake (Fig. 3c), contributed the altered clasts found in all 2007 lahar samples (Fig. 9a, 9b), thus providing a tracer for proximal bulking and downstream debulking. The -3Φ size class (0.5Φ interval) was the largest grain size analyzed for componentry. The proportions of altered clasts in the -3Φ size class range from 10% to 61% by mass (Fig. 10c), with an average of 31%. We take this average value as a proxy for the proportion of sediment that the landslide contributed to the lahar. It closely corresponds to the value of 29%, which Manville et al. (in review) calculated as the landslide contribution using LiDAR-derived elevation changes induced by the lahar. The consistency between these values suggests that deposits in the study area represent material sourced almost entirely from the upper gorge and that the lower gorge (>5 km from Crater Lake) contributed little material to lower gorge deposits. Altered clast abundances reach 41% by weight in the distal part of the study area, highlighting the transport capabilities of the 18 March 2007 lahar. However, the altered clast proportions generally decrease between 8 and 11 km from Crater Lake (Fig. 10d).

While the exact timing of the landslide was unclear prior to this study (Massey et al., 2009), the presence of large proportions of landslide components within all 2007 samples, including the deepest 2007M sample (38-09) collected at a depth of 300–400 cm, suggests that the landslide was activated during passage of the lahar body or earlier. However, the absence of clear trends in the proportions of altered clasts with deposit depth (Fig. 10e) indicates that landslide entrainment occurred frequently or continuously, probably coinciding with intermittent landslide damming and breaching in the lahar path (Massey et al., 2009). In the Whangaehu Gorge we assume that the landslide contributed the most significant volume of clays, generated through pre-lahar hydrothermal alteration. This assumption is consistent with the low clay content of historic lahar terraces (Table 2).

Systematic downstream changes in clay content have been used to calculate debulking factors and source clay contents of lahars, and to interpret the degree of hydrothermal alteration of an ancestral edifice (Cronin et al., 1997; Vallance and Scott, 1997). Such calculations are valid as long as clays are contributed near the source and downstream entrainment of additional clays is negligible (Vallance and Scott, 1997). Assuming that depositional styles neither prevented nor favored deposition of clay, the rate of clay loss as a function of distance can be used as a proxy for the loss of all material entrained upstream of the study area. This assumption appears valid locally, in the absence of turbulence, considering the inferred rapid vertical accretion of 2007M deposits that we interpret was induced by high intergranular friction (discussed in section 5.2.2). Although the proportion of landslide clays is unknown, a general downstream decrease in clay concentrations is recognized in the gorge (Fig. 8d), particularly for locations in the region of average debulking that begins 5 km from source (Manville et al., in review). Rapid rates of debulking indicated by the downstream decrease in clay content, however, necessitate additional bulking to maintain the average sediment loss rates of 0.67%/km between 5 and 11 km from source, found by Manville et al. (in review). The clay-based debulking rates would be far greater than those calculated by Manville et al. (in review). The disparity between these debulking rates may be explained by concurrent bulking of clay-depleted material (i.e., the 1975 and 1995 deposits), which would lower clay concentrations without debulking the flow. Such bulking may be particularly significant 8 to 11 km from source where six samples of the lowest clay concentrations were collected (Fig. 8d). Rapidly decreasing proportions of altered clasts over the same reach (Fig. 10d) provide additional evidence for locally rapid transitions between bulking and debulking regimes.

5.3 Stratification of the flow

The head of the side channel intersects the main channel 7 km from source at a sufficiently oblique angle and with a sufficiently steep drainage divide that the lahar most probably overflowed without significant ramping. It therefore experienced flow depths

no greater than the upper 47% of the flow calculated in section 4.1.1 (Fig. 6b). Although a dilute flow probably initially passed through the side channel during peak flow, the upper portion of the later main body of the lahar would have also passed through the side channel during the 1 hour 11 minute duration of overflow. Upon crossing the drainage divides, the dilute flow spread laterally, doubling in width, such that the maximum flow depth in the side channel probably did not exceed 3 m. The isolated, 80 cm thick, sandy 2007S deposits near the head of the channel (Fig. 5c) have weak cross stratification, indicating that their emplacement was associated with more turbulence than that of all four main channel 2007B lahar deposits. Such turbulence-dominated deposition is associated with low sediment concentration flows because greater sediment loads dampen turbulence (Smith, 1986; Costa, 1988). A dilute side channel flow is also consistent with the > 3 m net erosion in the side channel, because dilute flows are known to entrain material effectively (Cronin et al., 1999; Rodolfo et al., 1996).

These findings provide compelling evidence for a vertically stratified active lahar in the gorge at 7 km from Crater Lake during at least the first hour of the event. In addition to a sediment concentration that increases with depth, comparison of the sand modes in 2007S deposits and the main channel deposits (Fig. 7b) indicates that the grain size increase with depth is also significant. Although other studies have recognized the existence of density stratification (Hanes and Bowen, 1985; Bradley, 1986; Sohn, 1997; Cronin et al., 1997b; Manville and White, 2003; Pierson, 2005; Ghoshal and Mazumder, 2005), this study provides a direct comparison of the grain sizes transported in the upper half of the flow to those being deposited. Additionally the absence of clear trends in grain sizes of these deposits with depth (Figs. 8e, 8f, 8g) shows that grain size is not controlled by the competence of the waning stages of the side channel flow, ultimately suggesting that deposits are representative of the grain size distributions of the active flow. Direct dip techniques, rarely sampling a flow depth greater than 1 m, show that the uppermost transport region of hyperconcentrated flows dominantly carries sand (e.g. Pierson and Scott, 1985; Arboleda and Martinez, 1996; Cronin et al., 1997b). The grain size characteristics of the 2007S deposits demonstrate that even the middle depths of the 2007 flow primarily transported sand, with only scarce outsized clasts reaching 8 cm within the side channel. The basal layer that commonly develops in sediment-laden

33

flows has characteristics and behavior similar to those of denser debris flows (e.g. Pierson and Scott, 1985; Arboleda and Martinez, 1996; Cronin et al., 1997b), such that the 2007M deposits more closely resemble the basal flow than the entire flow profile (Pierson and Scott, 1985; Manville and White, 2003). Given that there is no evidence for a high sediment concentration flow in the side channel, the basal flow in the main channel appears not to have exceeded a thickness of 4 m, or half of total peak flow thickness at the overflow location 7 km from Crater Lake.

5.4 Abrasion and cataclasis

Our understanding of the internal flow dynamics of the 18 March 2007 lahar is improved through recognition of abrasion (clast rounding) and cataclasis (clast fracturing) that occurred during the event, particularly among altered clasts. These processes are recognized in lahars (cf. Vallance and Scott, 1997) and progressively reduce individual clast sizes and grain size distributions downstream, particularly during high-velocity flow (Schumm and Stevens, 1973). In this way, abrasion and cataclasis may impact the amount of sediment that can be transported within a sediment-laden flow because a greater volume of finer material can be transported under competence-limited conditions. Volume and density changes induced by debulking will impact upon flow velocity and consequently the destructive ability of the lahar (Fagents and Baloga, 2006). Abrasion and cataclasis occur in many sediment-laden flows, but are especially critical in lahars because volcanic sediment undergoes rounding up to an order of magnitude more quickly than non-volcanic material (Pearce, 1971). The fragility of highly weathered or altered clasts, such as the altered components of the 2007 lahar deposits, may accelerate this mechanical breakdown. For example, deposits of the 5.6 ka 3.8 km^3 Osceola mudflow at Mount Rainier contain a large volume of weak, hydrothermally altered components that show progressive downstream rounding. Additionally, 6 to 25% of Osceola clasts show breakage surfaces. Although the time taken for the lahar to reach the most distal location of our study area (11 km) may not have exceeded 20 minutes, individual clasts may have

still been subjected to abrasion and cataclasis by means of high lift and drag forces over much greater periods of time when blocking by other particles prevented particle movement (Schumm and Stevens, 1973) between cycles of entrainment and deposition.

Altered components within 18 March 2007 lahar samples, derived from highly angular landslide material 400 to 800 m from Crater Lake, show far greater rounding than unaltered components (Figs. 10a, 10b). Although rounding of altered components may be associated with the greater distance that this landslide-derived material traveled compared to terrace-derived material, unaltered components do not show a spectrum of rounding representing the variable transport distances. The only exceptions to the angularity of unaltered clasts are distinctly gray, rounded clasts that are interpreted to be landslide-derived, but fall in the unaltered category because they experienced sufficient abrasion and cataclasis to rid their surfaces of the yellow-to-red alteration used to define the altered classification. The accelerated abrasion of altered clasts is further highlighted by a comparison with the transport history of unaltered clasts, which are primarily derived from historic lahar deposits and may have undergone mechanical breakdown during multiple events. Altered clasts experienced abrasion only during the 2007 lahar event.

The 2007 lahar deposits have the highest matrix sand content and best rounding of all historic lahars, probably due to the high susceptibility of altered clasts to abrasion. Sediment sources for historic lahars have primarily been channel terraces, channel bed deposits, and fresh tephra. The incorporation and subsequent breaking of the landslide particles by the 2007 lahar may be responsible for producing the sand-dominated matrix. Although the 2007S side channel sample that was analyzed for 2Φ componentry (corresponding to the secondary mode of many 2007M deposits) has only 2-5% yellow-to-red grains consisting entirely of alteration material, the low amount of surface coverage of yellow-to-red alteration on -3.5Φ to -2Φ clasts suggests that the altered clasts lost significant volume by abrasion of the more heavily altered clast surface to produce sand-sized particles.

Whereas the high degree of rounding of altered clasts demonstrates abrasion, the marked reduction in altered clast abundances with decreasing grain size in all 2007

samples demonstrates cataclasis, and probably abrasion as well (Fig. 10c). Each time a clast is fractured and abraded during transport to produce two or more smaller clasts, there is a greater chance that one or more of the smaller clasts will not have the red alteration and will therefore be classified as unaltered. A fines-poor grain size distribution for the landslide material is also ruled out as a cause of the systematic trends because field observations note that the deposit had a matrix rich in fine gravel. One reason we find a scarcity of cleanly fractured surfaces on altered components is because cataclasis represents a high-magnitude, low-frequency size-reducing process, while abrasion is a low-magnitude, high-frequency processes, rapidly rounding angular clast edges. Although cataclasis of unaltered components is therefore difficult to track, additional fines may be produced by this mechanical process.

5.5 Generation of sand

Secondary modes of sand-sized particles are particularly abundant in the distal part of the study area and may represent particles generated by abrasion. Whereas cataclasis of a single grain can produce smaller grains of random sizes, abrasion is known to preferentially generate sand-sized grains from gravels (Jerolmack and Brzinski, 2010). Collision efficiency is reduced with decreasing gravel sizes (Schmeeckle et al., 2001), causing abrading parent gravels to approach a lower size limit and producing a bimodal grain size distribution with a gap in significant volumes of sediment of grain sizes between 0Φ and 4Φ diameters (Jerolmack and Brzinski, 2010). The bimodal Whangaehu Gorge 2007M and 2007B samples also demonstrate the lower gravel size limit, with the most abrupt decrease in weight percentage commonly occurring at approximately 10 mm diameter (Table 2) (3Φ to 4Φ). Troughs exist between modes of 1 and 4 mm diameter (0Φ to -2Φ). Increased volumes of sand generated by abrasion are represented by secondary modes between 0.5 and 0.25 mm diameter (1Φ to 2Φ) (Fig. 9), which consist primarily of free crystals, indicating that phenocryst sizes within parent gravels may also control the size of abrasion-generated grains. Although there is a minimal abundance of

yellow-to-red altered material in the 2Φ category, the evidence for the occurrence of abrasion and cataclasis deeper within the clasts than the surficial alteration suggests that altered clasts may also generate crystalline sand.

The rapid vertical accretion inferred for the 2007M deposits probably preserves the abraded sand better than stream flow deposits. During dilute flow, gravel bed rivers commonly carry the abraded sand in suspension, while larger gravel clasts are transported by saltation nearer the bed surface (Jerolmack and Brzinski, 2010). However, the high density flow that emplaced the 2007M deposits dampened turbulence in the basal flow. It prevented significant volumes of sand, produced by intergranular friction, from escaping the basal flow. Dampened turbulence may have also caused downward percolation of fines through voids between coarse clasts in the active flow. This process is known to occur in flows with sediment concentrations above 40% by volume (Vallance, 2000). The basal flow of the 18 March 2007 lahar probably exceeded this limit, so percolation may have been a mechanism by which sand reached the depositing layer of the basal flow. Rapid, non-selective deposition subsequently preserved the sand, which are represented by secondary modes. Mass percentages of secondary modes were calculated as the difference between the mass of the entire secondary mode and the mass if the grain size distribution followed a unimodal Gaussian curve, and reach 8% by weight (Table 2, sample 40-01). This quantity represents the minimum mass of sand generated by abrasion within the flow by the time of deposition. Grain sizes of 2007M secondary modes nearly match those of 2007S side channel deposits, indicating that increased turbulence upwards in the stratified flow allowed sand to reach the transport region. Therefore significant masses of sand may have been transported downstream of the study area, suggesting that sand generated during the event exceeds masses represented by secondary modes.

5.5.1 Variability of sand content with distance

The development of sand-sized secondary modes is associated with the evolution of high density lahars at many volcanoes (cf. Vallance and Scott, 1997; Capra et al., 2004;

Castruccio et al., 2010). A lahar in 1997 on Popocatépetl volcano in Mexico was generated similar to the 2007 Whangaehu lahar by a sudden release of water. The Popocatépetl deposits also show secondary modes centered at 2Φ at intermediate distances from the source (Capra et al., 2004). Secondary modes may only have been preserved in deposits after bulking sufficiently increased the sediment concentration to enhance intergranular collisions to produce sand and emplace it in massive deposits. A series of lahars in 1961 on Calbuco volcano in southern Chile, on the other hand, were generated when pyroclastic flows overran snow and ice.   Dilution led to the distal emplacement of coarse-grained, matrix-supported deposits with 1Φ to 3Φ secondary modes (Castruccio et al., 2010). The Calbuco secondary modes may only have been produced by abrasion and cataclasis once a sediment concentration was reached that was low enough to enhance flow mobility but high enough for intergranular friction to produce sand. The 5.6 ka Osceola mudflow at Mount Rainier, Washington also rapidly increased in flow mobility after the source edifice failure, showing progressive increases in intensity of 2Φ (medium sand) secondary modes up to 100 km from source (Vallance and Scott, 1997).

The mass fraction of sand per sample from the Whangaehu Gorge main channel also generally increases with distance, but recognizable correlations of grain size with distance are apparent only for fine sand and medium sand (Fig. 8c), which approximately double in mass fraction over the study area 5 to 11 km from source. The absence of other grain size trends with distance, particularly in silt and finer grain sizes, together with generally stable primary modes, suggests that sand was indeed preferentially generated by abrasion and cataclasis. By 39 km from Crater Lake, deposits developed a sand-sized unimodal grain size distribution with improved sorting, centered at 2Φ, demonstrating both the high volumes of sand that had been generated by abrasion/cataclasis and the reduction in flow competence at this distance.

5.5.2 Variability of sand content with depth

Greater sand abundance with depth in the deposit suggests that the earlier stages of deposition generated more sand through more efficient abrasion and cataclasis. For each of the three locations from which two samples were acquired with no overlapping sample depths, the deeper of the two samples shows a coarser primary mode and a more pronounced secondary mode, while maintaining the same general grain size distribution pattern as the shallower sample (Fig. 7c). Samples 40-01 and 40-02 most clearly demonstrate the striking similarity in grain sizes of secondary modes, and these samples also show the amplification of the secondary mode with depth (Table 2). Coarser primary modes at greater depth indicate that increased flow competence early in lahar evolution may have caused intergranular collisions of greater force to produce more sand. Additionally, the expected higher flow density earlier in lahar evolution (Fig. 2a) may have caused more frequent intergranular collisions to produce more sand, and retain more sand in the basal flow under dampened turbulence conditions, while providing conditions favorable for percolation of sand (cf. Vallance, 2000) down to the depositional base of the flow.

5.5.3 Impacts of external sediment

Other studies have attributed the development of sand-sized secondary modes to entrainment of external sediment sources (cf. Kodama, 1994; Vallance and Scott, 1997; Castruccio et al., 2010). However, 1Φ to 2Φ secondary modes in the 2007 deposits exist despite the absence of any material with 1Φ to 2Φ primary modes that was contributed to the lahar before or during emplacement of bimodal deposits. This supports our interpretation that sand was generated by internal flow dynamics during the 18 March 2007 event. Historic lahar terraces contributed the most sediment to the flow (Manville et al., in review), but have sand abundances no greater than 2007 lahar main channel deposits (Table 2). The only pre-lahar sand-sized material in the Whangaehu Gorge exists in the side channel, including alluvium (primary mode: 3Φ) and fluvial sediment (primary mode: 0Φ), but termination of side channel activity after 1 hour 11 minutes

suggests that the late-stage deposits with secondary modes were not affected by this contribution. Additionally, 2007 lahar deposits with secondary modes exist upstream of the side channel. Pre-lahar main channel bedload sediment was observed to have a primary mode greater than 2Φ, and an incisional period during the twelve years prior to the event prevented significant accumulation of fine grained deposits from base stream flow.

Secondary modes in the Whangaehu Gorge 2007 deposits are least pronounced in deposits that show the most significant bulking prior to deposition and are most pronounced in deposits that show the least significant bulking prior to deposition, based on volumetric analysis for the degree of bulking. This indicates that internally generated sand is best recorded as secondary modes in deposits that experienced minimal contributions of external sediment prior to emplacement, which would otherwise have decreased the relative proportions of sand. Volumetric analysis shows that the amount of material eroded by the flow is greatest in the proximal gorge, decreasing nearly exponentially from 1.2 to 5.0 km before sharply dropping off at 5.2 km and fluctuating at low volumes further downstream (V. Manville unpublished data). For example, samples 23-01 and 23-02 show negligible secondary modes, although they are the most proximal samples (4.9 km), with 6,000 m^3 of erosion in a 100 m reach that included this sample location, and up to 8,000 m^3 of erosion in a 100 m reach located 500 m upstream of the sample site. Sample 40-01, on the other hand, has the most pronounced secondary mode, but there is only 500 m^3 of erosion in the sampled 100 m long reach and no more than 1500 m^3 of erosion per 100 m in the upstream 500 m (V. Manville unpublished data). Between 5 and 9 km the most pronounced secondary modes also progressively intensify (Fig. 12a). While reduced bulking allows more pronounced secondary modes to be recognized with distance, greater durations of abrasion and cataclasis downstream also increase sand content. Similarly to volumetric erosion, erosion depths are shallowest in gorge locations where deposits have the most pronounced secondary modes (Fig. 12b). The trend that samples with the most pronounced secondary modes have the lowest clay contents shows that bulking is not responsible for the secondary modes (Fig. 12c). Instead, significant bulking masks the sand-sized secondary modes generated by abrasion and cataclasis in the Whangaehu Gorge.

CHAPTER 6. DISCUSSION

A spatiotemporally multi-dimensional approach was possible in this study due to the extensive pre- and post-lahar monitoring efforts, and these provided insights into the relationships between lahar sediment concentration, depositional style, deposit character, and ultimately internal flow dynamics of sediment-laden flows. Figure 11 illustrates the evolution of these properties during the 18 March 2007 lahar. Peak total discharge preceded peak sediment discharge, resulting in a highly erosional regime (Fig. 11a). The generation of sand-sized particles occurred during peak sediment discharge when intergranular collisions were most frequent and involved the greatest momentum. High sediment concentration and dampening of turbulence in the basal flow was greatest at this time (Fig. 11b), causing emplacement of thick, massive deposits with the most pronounced secondary modes of sand-sized material (Fig. 11c). As the body of the flow passed, sediment concentration waned (Fig. 11a), turbulence in the basal flow increased (Fig. 11b), and a competence-limited depositional regime was responsible for periodic selective deposition of the largest clasts in clast-supported lenses (Fig. 11c). With further reduced sediment concentration, the onset of significant turbulence was responsible for bedded deposits (Fig. 11c).

Classifications of flow types, including hyperconcentrated flow and debris flow, are based on solids content (Beverage and Culbertson, 1964), and have been used to describe differences in turbulence and rheology, which impact depositional style and deposit character (cf. Smith, 1986; Costa, 1988; Iverson, 1997; Major, 1997; Vallance, 2000). However, except for the most dense flows, lahars generally demonstrate nonlinear sediment concentration gradients (cf. Hanes and Bowen, 1985; Bradley, 1986; Sohn, 1997; Cronin et al., 1997b; Manville and White, 2003; Pierson, 2005; Ghoshal and Mazumder, 2005), making the estimation of sediment concentrations and flow properties over the depth of a lahar a challenge. Volumetric sediment flux analysis of the 2007 Whangaehu lahar provided time-averaged sediment concentrations by comparing pre- and post-lahar airborne LiDAR topographic data. The calculated average sediment concentrations ranged from 51% by volume in the upstream-most reach 5 km from Crater Lake to 47% in the downstream-most reach of the study area (Manville et al., in review).

The lower limit for debris flow classification is 60% by volume (Beverage and Culbertson, 1964). However, the vast majority of 2007 Whangaehu Gorge deposits are matrix-supported, very poorly sorted, and seldom show bedding; these characteristics are most commonly attributed to debris flow concentrations (Vallance, 2000). A basal flow with behavior similar to that of a debris flow (Fisher, 1983) is probably responsible for these deposits. The vertical scale of stratification in the flow is constrained by side channel deposits that correspond to the dilute transport region of the lahar, which represents at least the upper 4 m of the flow at peak stage. Furthermore, the height of the overspill above the main channel suggests that the basal flow occupied the lower 50%, or less, of the lahar. Minimal deviation with depth from a coarse sand mode in the side channel deposits, emplaced as stage height waned, indicates that the upper half of the lahar had only a subtle density gradient and that the strongest gradient exists in a narrow zone immediately above the basal flow (Fig. 11b).

The disparity between deposit character and time-averaged sediment concentration additionally underscores the temporal variability in solids content associated with a clear-water breakout event such as the lahar of this study. The early, dilute stages of such lahars rapidly bulk with external sediment (Cronin et al., 1999; Rodolfo et al., 1996) before peak discharge, after which maximum sediment concentration is reached. Next, with waning discharge and a limit to the capacity of the lahar to hold sediment (cf. Hiscott, 1994), debulking ensues. Manville et al. (in review) demonstrated that time-averaged sediment concentrations decreased with distance in the study area (5–11 km from source), however these numbers have limited sedimentological relevance. In contrast, we are able to establish an understanding of time-dependent flow concentrations of the 2007 lahar from the range of deposit types, and therefore depositional styles, that change with depth in the Whangaehu Gorge. The deepest deposits, i.e., the massive, matrix-supported 2007M deposits, show no trends between grain size statistics of coarse clasts and depth, confirming that it was not waning competence that caused deposition, but instead waning capacity. Additionally, deposits are strongly matrix-supported and even bimodal, indicating non-selective deposition, probably during rapid vertical accretion induced by friction between the unsorted basal flow and the channel bed (Major, 1997). Primary and secondary modes in the deepest of

these deposits are, however, coarsest and most pronounced, respectively, indicating decreasing basal flow sediment concentration with time. As debulking continued, and sediment concentration and total discharge waned (Fig. 11a), flow competence became the limitation which, in conjunction with reduced yield strength (Pierson and Costa, 1987), allowed the largest clasts to preferentially settle out from transport (Baker and Ritter, 1975) and accumulate incrementally (cf. Vallance, 1994) to form the clast-supported lenses. The isolated nature of these deposits, found interbedded between matrix-supported deposits, suggests that the transition to a competence-limited regime is subtle and fluctuating; the unsteady, surging nature of the lahar discharge (Fig. 6b) may be responsible. Stratigraphically shallowest, the 2007B bedded deposits are indicative of a temporal transition to a more dilute, turbulence-dominated flow regime. The deposits show increasing clast sizes with depth, suggesting that the expected competence limitation was maintained until the event ceased.

Abrasion is known to produce sand-sized secondary modes in many gravel bed rivers due to the preferential mechanical breakdown to grains finer than 0Φ, without entrainment of external sediment (Kodama, 1994; Jerolmack and Brzinski, 2010). The abundance of sand in lahar deposits has also been attributed to the incorporation of external sediment during flow emplacement (Vallance and Scott, 1997; Rădoane et al., 2008). Vallance and Scott (1997) suggest that increasing bimodality with distance may be due to either bulking of two distinct sediment populations or a bimodal source such as alluvium. However, they provide neither evidence for sources with these grain size distributions nor evidence for sustained downstream bulking that would cause the secondary modes to become amplified up to 100 km downstream. Rădoane et al. (2008), however, compare grain size distribution patterns of external sediment to those of river sediment upstream of entrainment to show that the downstream grain size distributions are a combination of the two sediment populations. With comprehensive grain size distribution patterns for both primary deposits of the 18 March 2007 lahar and all potential external sediment contributions, we were able to identify the origin of secondary modes as abrasion and cataclasis with sand-sized secondary mode development in the reaches with the least bulking. Most importantly, the absence of any sand-sized external sediment contributions suggests that sand-sized clasts represent the

production and preservation of sand by abrasion and cataclasis during this single event.
Future research on sediment-laden flow dynamics may similarly benefit from
interdisciplinary studies between the fluvial geomorphology and lahar communities.

CHAPTER 7. CONCLUSIONS

Spatiotemporal variability in the flow characteristics and behavior of the 18 March 2007 lahar are preserved in deposits that pass from coarse-grained, matrix-supported units to finer-grained, clast-supported units, and finally to stratified units at the top of the deposit. This progression from a capacity-limited, turbulence-dampened depositional regime to a turbulence-driven depositional regime provides insights into time-dependent changes in flow density (solids concentration), which has commonly been calculated as a time-average over the duration of the flow. Depositional styles, interpreted in this study from comprehensive grain size analyses and bedding and grading characteristics, reflect the density of the basal flow as well as the capacity- versus competence-limitation of the flow. Massive deposits enriched in sand and emplaced under capacity-limited conditions represent the most accurate snapshot of the basal flow. While time-averaged solids concentrations would predict that the event was a hyperconcentrated flow with sediment concentrations of 46–51% in the study area 5–11 km from source (Manville et al., in review), deposits emplaced over an extended period show that peak sediment concentrations were well into the debris flow classification. The discrepancy between time-averaged sediment concentration and deposit character reflects the depth-dependent solids concentration of the flow. This study shows that the 2007 lahar flow profile has a strong density gradient that changes from a high density gravel-rich basal flow to a dilute transport region carrying dominantly sand. The sand fraction was generated during the event by abrasion and cataclasis, particularly during the early, most concentrated stages of lahar evolution.

TABLES

Table 1. Samples and associated field attributes. Sample colors correspond to those used in Fig. 4. *Minimum deposit thickness represents the elevation change during the event, due to both erosion and deposition (i.e. negative values reflect net erosion).

Sample	Deposit	Grading	Sample Depth (cm)	*Min deposit thickness (cm)	Distance (km)	Comments
18	1995	Massive	150 – 75		6.4	Abundant highly rounded cobbles and boulders.
19	2007	Bedded	0 – 100	-18	6.2	Clast-supported gravel lenses laterally extensive (not sampled).
21	2007	Massive	67 – 99	212	5.7	Fines-rich top (not sampled).
22	Landslide	Massive	0 – 100		0.7	Clasts are highly angular with yellow-to-red alteration. Matrix-bearing.
23-01	2007	Massive	50 – 100	-148	4.9	Sample is from lower half of uppermost terrace of three.
23-02	2007	Massive	0 – 50	-148	4.9	Continuous deposit with sample 23-01. Sample is from upper half of terrace.
24	2007	Massive	20-120	278	9.3	
28-02	2007 Side channel	Bedded	11-18	80	7.2	
28-04	2007 Side channel	Bedded	40-43	80	7.2	Weak, low-angle, cross stratified, silty-sand deposit.
28-05	2007 Side channel	Bedded	52-58	80	7.2	Weak, low-angle, cross stratified, silty-sand deposit.
28-07	2007 Side channel	Bedded	70-80	80	7.2	Bouldery, framework supported gravel with 60 cm boulder.
29	Alluvium	Bedded	0-100		7.3	Thickest expanse of alluvial slope waste that has contributed bulk to flow.
31	Fluvial sediment	Cross-bedded	0-50		7.4	Cobbly bar deposit overlain by muddy matrix-rich xbedded deposit.
34	2007	Bedded	0-60	-67	10.6	
35-01	1975	Massive	0-52		7.6	
35-02	Coarse alluvium	Massive	0-50		7.6	
36	2007	Massive	0-60	4	7.7	
37	2007	Massive	50-100	307	6.7	
38-08	2007	Massive	100-200	581	6.4	The overlying unit consists of long wavelength cross lenses of better sorted gravel.
38-09	2007	Massive	300-400	581	6.4	Same location, greater depth than sample 38.
39	2007	Massive	0-200	7	6.0	
40-01	2007	Massive	90-140	122	8.6	
40-02	2007	Massive	50-90	122	8.6	Interbedded lenses of well-sorted gravel. Sample overlain by bar and ridge forming clast-supported
41	2007	Bedded	0-25	-67	10.6	Sample taken from bench. Unusually yellow-brown oxidation in matrix.
42	1975	Bedded	0-60		9.8	Deposit crudely lenzoid, bedded on 10-20 cm scale, defined by fluctuations in abundance of sand-sized
43	2007	Bedded	0-40	-59	11.1	
44	2007	Massive	0-50	-111	10.9	
45	1975	Massive	250-400		8.8	
46	1995	Massive	0-150		7.2	Significant number of angular blocks resembling local lava.
47	1995	Massive	0-150		7.9	Framework of large boulders and pockets of sandy pebbly matrix.

Table 2. Samples, associated grain size distribution characteristics, and histograms. Mean, sorting, skewness, and kurtosis are all based on the Folk and Ward (1957) method. Histograms are logarithmic with Φ on the x-axis and class weight percentage on the y-axis. Secondary mode height represents the height between the trough and the peak. D_x values represent the grain size at which a specified percentage of grains are coarser.

Sample	Deposit	Grading	Sample Depth (cm)	Distance (km)	Mean (φ)	Sorting (φ)	Skewness (φ)	Kurtosis (φ)	Primary Mode (φ)	Secondary mode (φ)	Secondary mode height (wt. %)	D_{10} (φ)	D_{50} (φ)	D_{90} (φ)	(D_{90}/D_{10}) (φ)	Grain size distribution
18	1995	Massive	150 – 75	6.4	6.48	2.15	0.44	1.42	-	-	-	-8.46	-6.90	-2.99	0.35	
19	2007	Bedded	0 – 100	6.2	4.45	3.30	0.04	1.01	-8.5	1	0.38	-8.41	-4.34	0.25	-0.03	
21	2007	Massive	67 – 99	5.7	3.56	2.19	0.33	1.02	-4.5	-	-	-5.83	-3.97	-0.23	0.04	
22	Landslide	Massive	0 – 100	0.7	-	-	-	-	-	-	-	-	-	-	-	
23-01	2007	Massive	50 – 100	4.9	6.02	2.37	0.25	1.16	-7.5	-2	0.28	-8.47	-6.18	-1.97	0.23	
23-02	2007	Massive	0 – 50	4.9	5.80	2.18	0.10	1.02	-6.5	-	-	-8.37	-5.81	-2.84	0.34	
24	2007	Massive	20-120	9.3	5.07	2.96	0.41	1.19	-6.5	2	0.53	-7.94	-5.74	0.08	-0.01	
28-02	2007 Side channel	Bedded	11-18	7.2	0.43	2.38	0.19	1.04	-0.5	-	-	-3.11	-0.61	2.89	-0.93	
28-04	2007 Side channel	Bedded	40-43	7.2	0.04	1.59	0.21	1.25	-0.5	-	-	-1.74	-0.10	2.24	-1.29	
28-05	2007 Side channel	Bedded	52-58	7.2	1.16	1.61	0.15	1.46	0.5	-	-	-0.68	1.02	3.24	-4.74	
28-07	2007 Side channel	Bedded	70-80	7.2	1.72	2.30	0.15	0.96	-1.5	-	-	-4.38	-1.83	1.50	-0.34	
29	Alluvium	Bedded	0-100	7.3	0.75	2.02	-0.10	0.84	2.5	-	-	-1.92	0.91	3.20	-1.66	
31	Fluvial sediment	Cross-bedded	0-50	7.4	0.03	1.99	-0.08	1.03	-0.5	-	-	-2.65	0.02	2.44	-0.92	
34	2007	Bedded	0-60	10.6	6.91	1.55	0.31	1.10	-7.5	-	-	-8.58	-7.16	-4.52	0.53	
35-01	1975	Massive	0-52	7.6	4.88	2.51	0.38	1.78	-5.5	-	-	-7.25	-5.24	-0.46	0.06	

Table 2. (Continued) Samples, associated grain size distribution characteristics, and histograms.

Sample	Deposit	Grading	Sample Depth (cm)	Distance (km)	Mean (φ)	Sorting (φ)	Skewness (φ)	Kurtosis (φ)	Primary Mode (φ):	Secondary mode (φ)	Secondary mode height (wt. %)	D10 (φ):	D50 (φ):	D90 (φ):	(D90/D10) (φ):	Grain size distribution
35-02	Coarse alluvium	Massive	0-50	7.6	6.14	1.83	0.29	1.31	-7.5	-	-	-7.86	-6.29	-3.67	0.47	
36	2007	Massive	0-60	7.7	4.48	1.84	0.19	1.28	-4.5	-	-	-6.61	-4.62	-1.76	0.27	
37	2007	Massive	50-100	6.7	4.36	3.20	0.26	1.01	-7.5	1	0.53	-7.85	-4.83	0.56	-0.07	
38-08	2007	Massive	100-200	6.4	5.01	2.83	0.19	1.17	-4.5	-	-	-8.09	-5.12	-0.89	0.11	
38-09	2007	Massive	300-400	6.4	4.53	3.26	0.35	0.97	-7.5	1	1.18	-8.00	-5.30	0.53	-0.07	
39	2007	Massive	0-200	6.0	4.04	3.00	0.50	1.20	-5.5	1	0.91	-6.89	-5.02	0.83	-0.12	
40-01	2007	Massive	90-140	8.6	4.97	2.86	0.63	1.37	-6.5	2	2.73	-7.52	-6.12	0.67	-0.09	
40-02	2007	Massive	50-90	8.6	5.78	1.27	0.12	1.26	-5.5	2	0.39	-7.28	-5.81	-4.09	0.56	
41	2007	Bedded	0-25	10.6	5.72	2.53	0.53	1.48	-6.5	2	2.08	-7.77	-6.30	-0.16	0.02	
42	1975	Bedded	0-60	9.8	4.04	2.82	0.11	0.98	-3.5	-	-	-7.32	-4.07	0.19	-0.03	
43	2007	Bedded	0-40	11.1	3.96	3.12	0.39	0.97	-6.5	2	0.75	-7.22	-4.74	1.06	-0.15	
44	2007	Massive	0-50	10.9	4.83	2.91	0.55	1.24	-6.5	2	1.19	-7.54	-5.81	0.50	-0.07	
45	1975	Massive	250-400	8.8	4.28	3.26	0.27	0.88	-7.5	-3	2.36	-7.75	-4.71	0.77	-0.10	
46	1995	Massive	0-150	7.2	5.65	3.27	0.60	0.80	-8.5	-3	1.36	-8.69	-7.01	-0.17	0.02	
47	1995	Massive	0-150	7.9	5.50	3.52	0.71	0.70	-7.5	-1	5.65	-8.66	-7.33	0.28	-0.03	

FIGURES
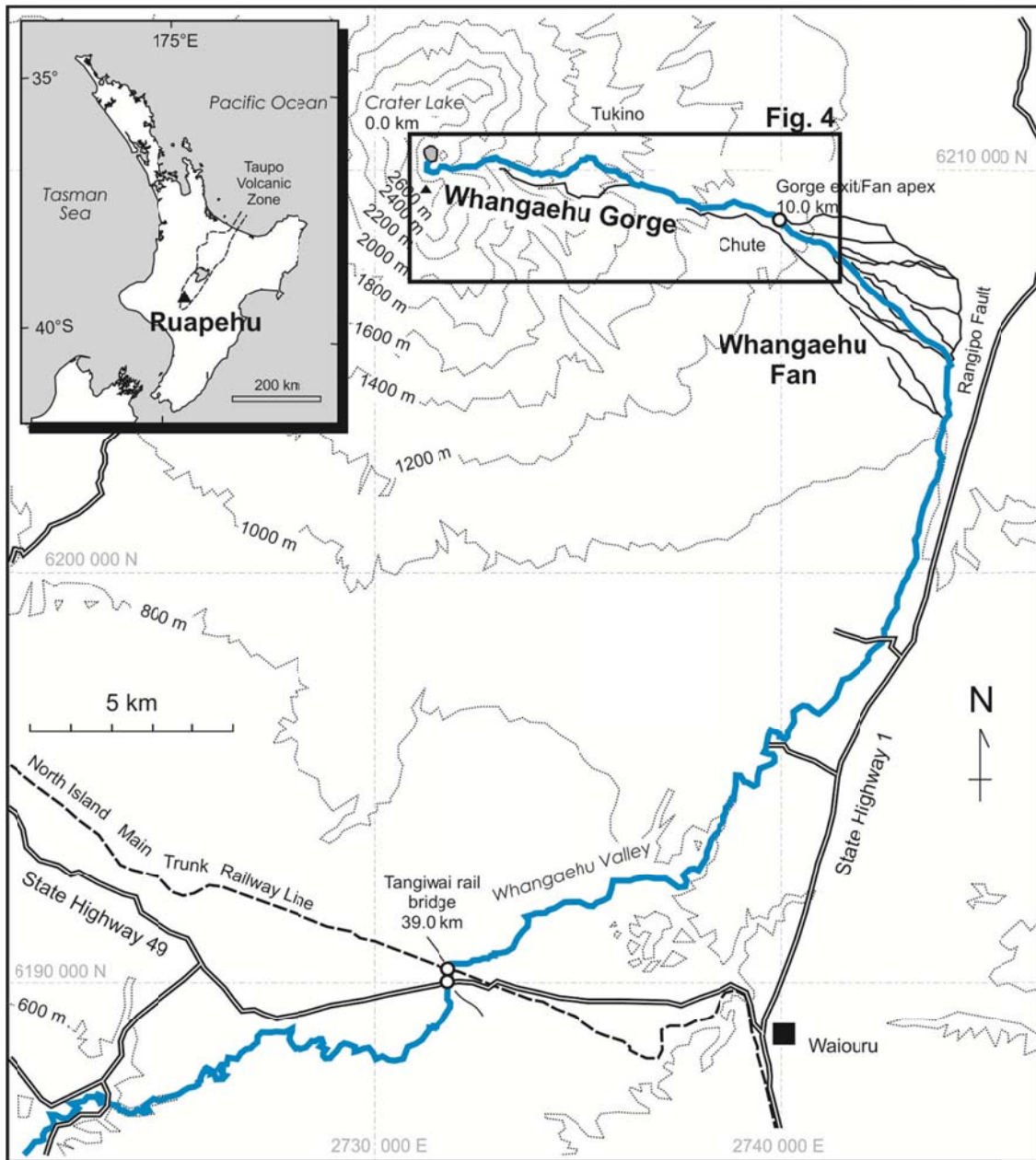
Fig. 1 Location map of the 18 March 2007 Mount Ruapehu lahar path (in blue). Boxed area shows the field area of Fig. 4. Grid references are in NZMG 260 series. (Adapted from Graettinger et al., 2010.)
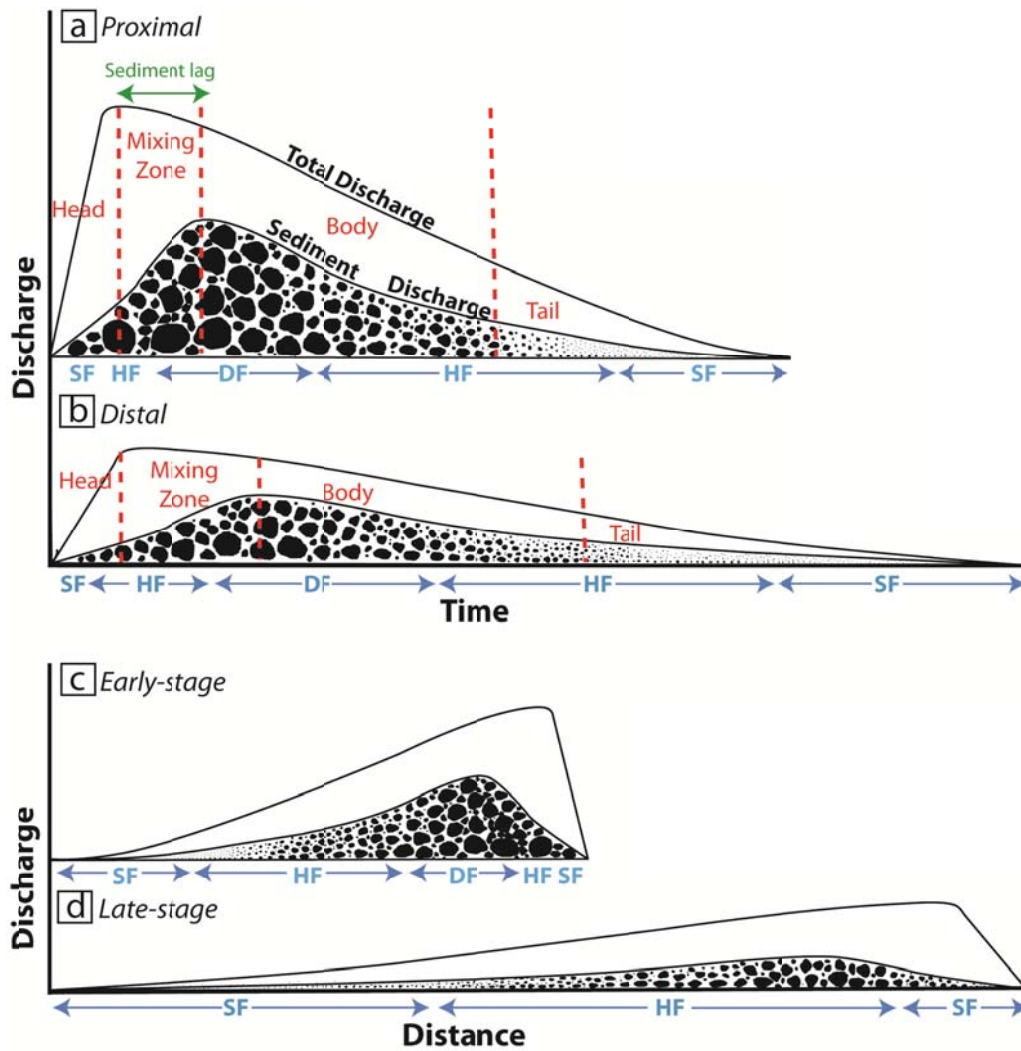
Fig. 2 Schematic representation of total discharge and sediment discharge as a function of time at a proximal location (**a**), and a distal location (**b**), and as a function of distance from source (**c**) shortly after the onset of the lahar; and (**d**) after more time elapsed. The proportion of the vertical profile covered by sediment discharge indicates the sediment concentration by volume; it is not an indication of segregation of the liquid and sediment components. SF = streamflow, HF = hyperconcentrated flow, DF = debris flow. Sediment lag indicates the duration between peak total discharge and peak sediment discharge.

50
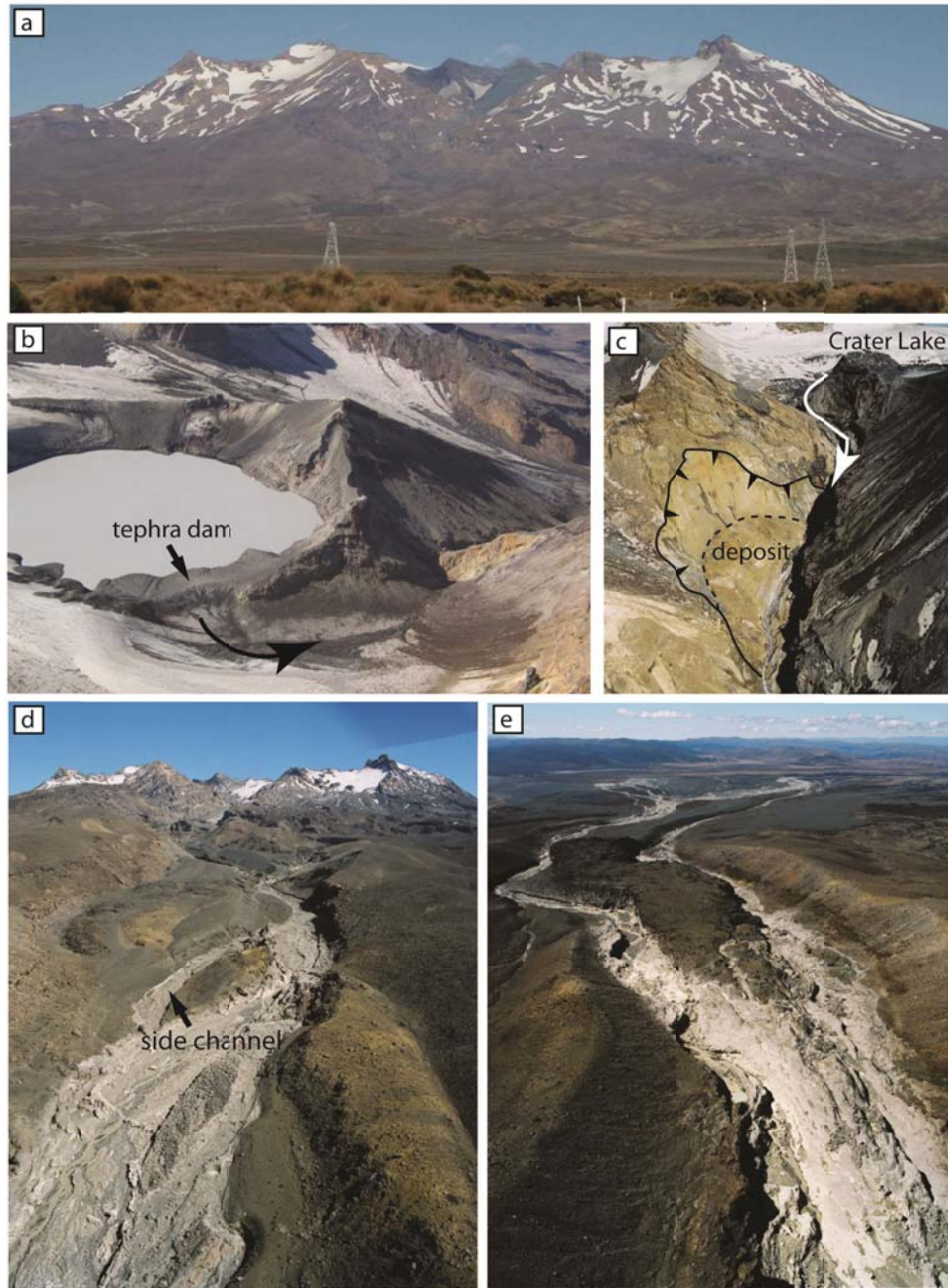
Fig. 3 a Mount Ruapehu. **b** Crater Lake and the upper Whangaehu Gorge viewed from the SW. **c** Landslide on the upper Whangaehu Gorge 400–800 m downstream of Crater Lake viewed from the E. **d** Whangaehu Gorge viewed upstream, 8 km from Crater Lake. Light-colored deposit indicates the flow inundation area of the 18 March 2007 lahar. **e** Whangaehu Gorge viewed downstream, 9 km below Crater Lake. (photo **b** – **e** courtesy V. Manville)

51
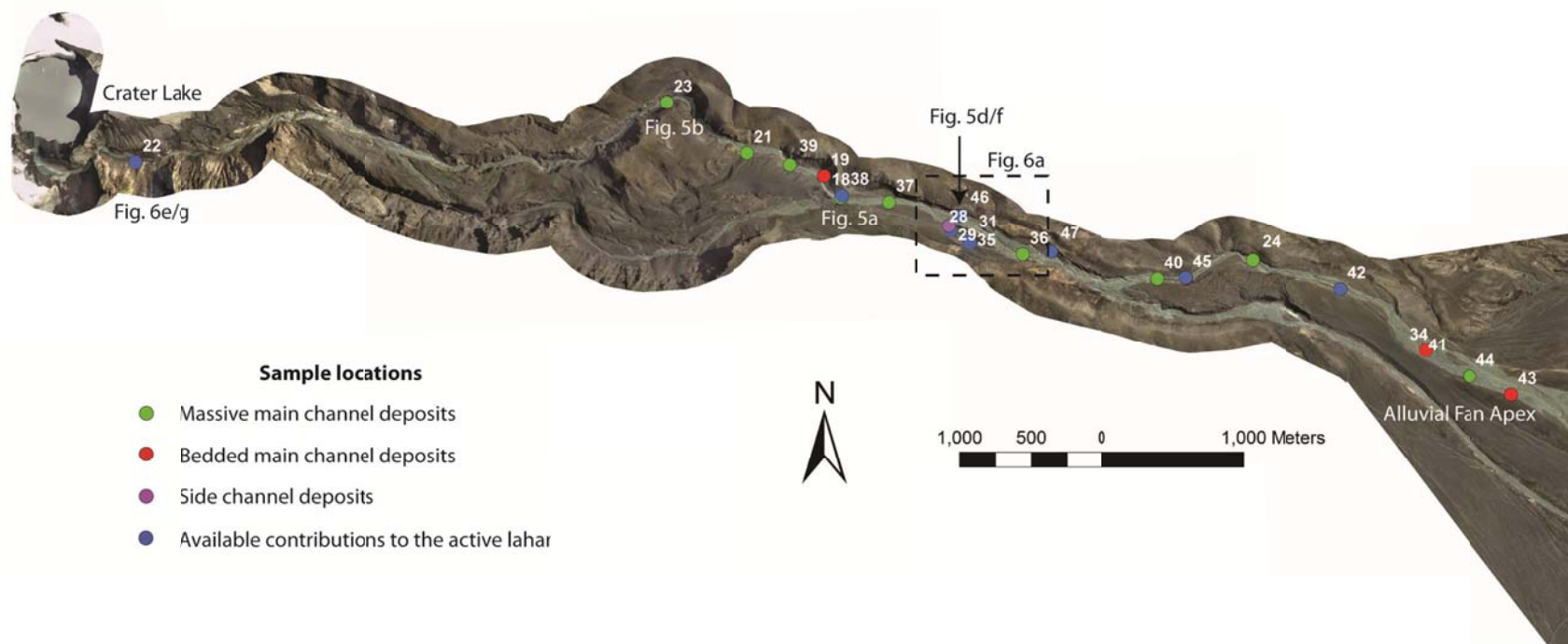
Fig. 4 Orthometric photograph of the Whangaehu Gorge study region with sample locations of primary deposits from the 18 March 2007 lahar and deposits that may have contributed to the lahar from Crater Lake (left) to the alluvial fan apex (right). (Orthophotograph courtesy V. Manville.)
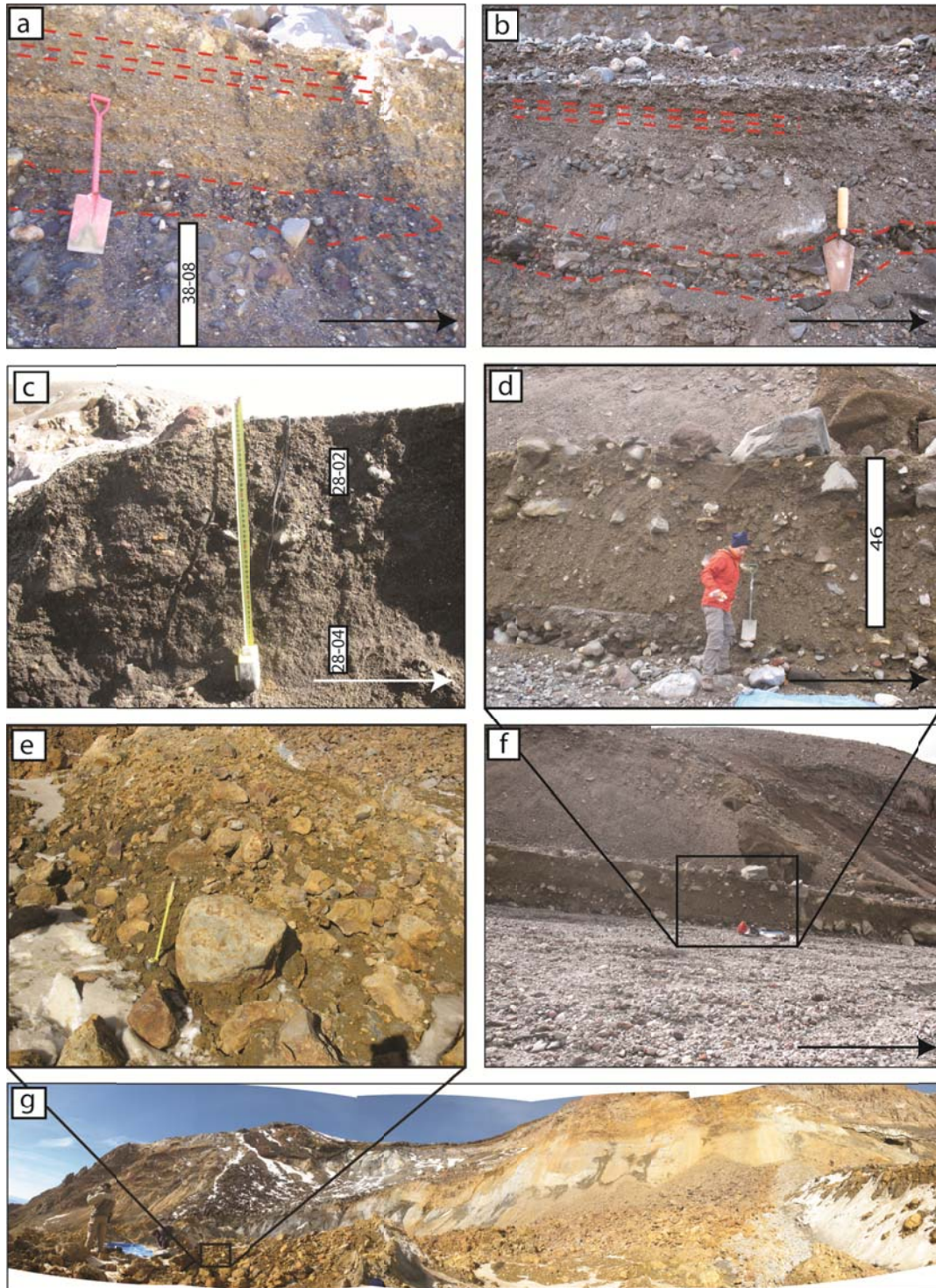
Fig. 5 Primary deposits and contributing deposits of the 18 March 2007 lahar with arrows indicating flow directions and bars indicating sampled depths and sample number. **a** (6.4 km from Crater Lake) **and b** (4.9 km) show 2007M lahar deposits that are massively bedded and overlain by clast-supported lens (between lower dashed lines) and a finer-grained, weakly bedded unit (parallel dashed lines above). **c** (7.2 km) Upper 50 cm of the side channel deposits. **d and f** (7.2 km) 1995 lahar terrace that provided erosional material for the 2007 lahar. **e and g** landslide deposit 400–800 m from Crater Lake (out of view to the right).
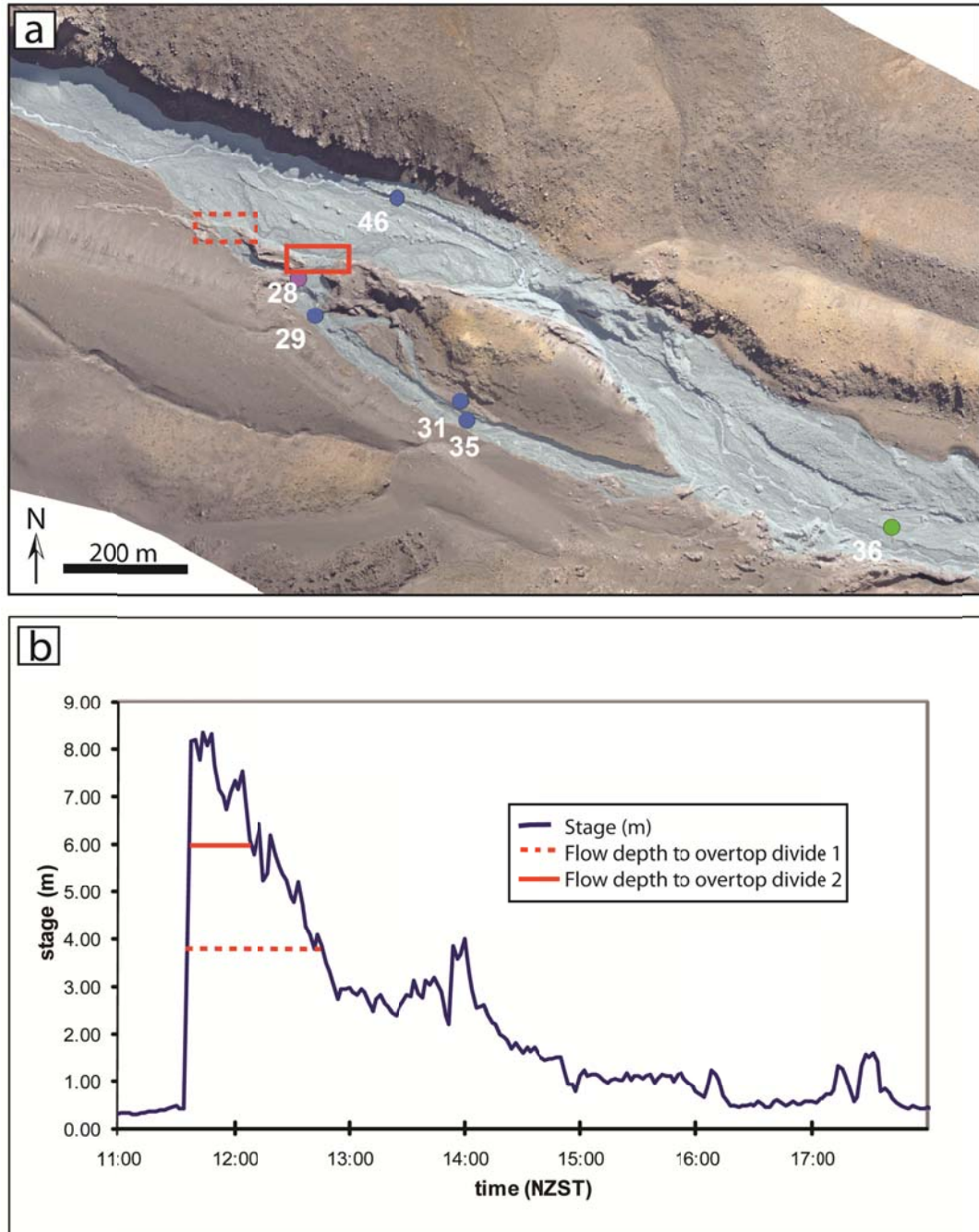
Fig. 6 a Side channel, south of the main channel in orthophotograph (courtesy V. Manville), 7.2 km from Crater Lake showing two drainage divide locations (boxes) overtopped by the lahar in the main channel, inundation area in transparent blue (A. Graettinger), and locations of 2007S samples (28) and alluvial/fluvial/1975 lahar deposit samples (29, 31, 35). **b** Stage vs. time (courtesy V. Manville) from stage gauge 7.3 km from source along the main channel. Dashed and solid lines show the heights above the main channel required for overflow into the side channel. Durations of overflow at these levels are shown by the length of solid and dashed lines. The upstream divide was 3.9 m above the pre-lahar main channel floor, allowing the upper 4.4 m of the flow top to enter the side channel. The downstream divide was 6.0 m above the pre-lahar main channel, allowing the upper 2.3 m of the flow to enter the side channel.

54
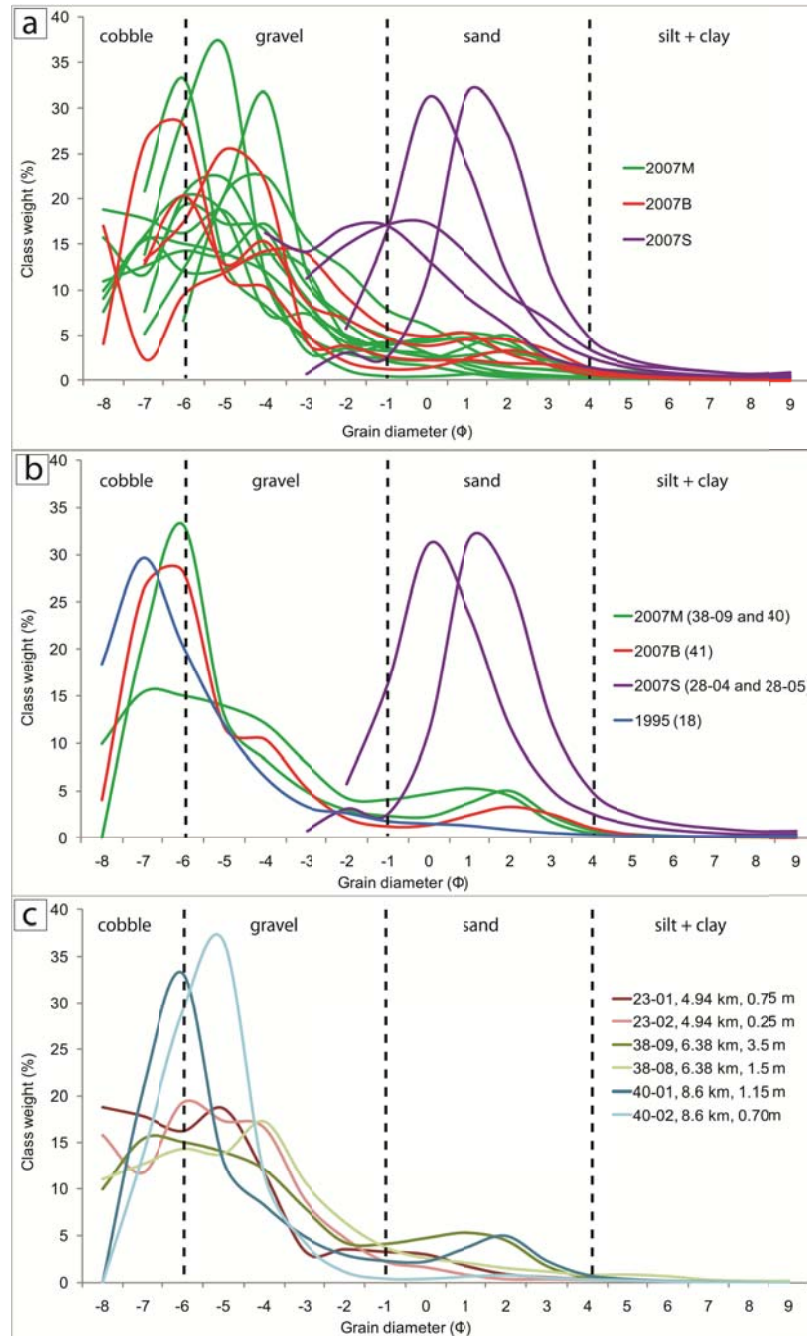
Fig. 7 Grain size vs. weight % for selected samples, smoothed from histograms. **a** All 2007 lahar samples. **b** Representative samples of the three 2007 lahar deposit types and a1995 terrace that is the most abundant bulking material in the region. **c** Three pairs of 2007M samples from different depths at the same locations. Sample pairs are the same color with a lighter shade designating the shallower sample. Note that samples from the same location have more similar grain size distribution patterns than any two samples from different locations. All three deeper samples have greater weight percentages of cobbles and sand, coarser primary modes, but lower weight percentages of gravel than their shallow counterparts. Two deeper samples (23-01 and 38-09) have well defined secondary modes compared to the shallower samples (23-02 and 38-08) from the same location with no secondary modes. The third deeper sample (40-01) has a very well defined secondary mode at 2Φ compared to the shallower sample (40-02) that has only a very weakly defined secondary mode at 2Φ.
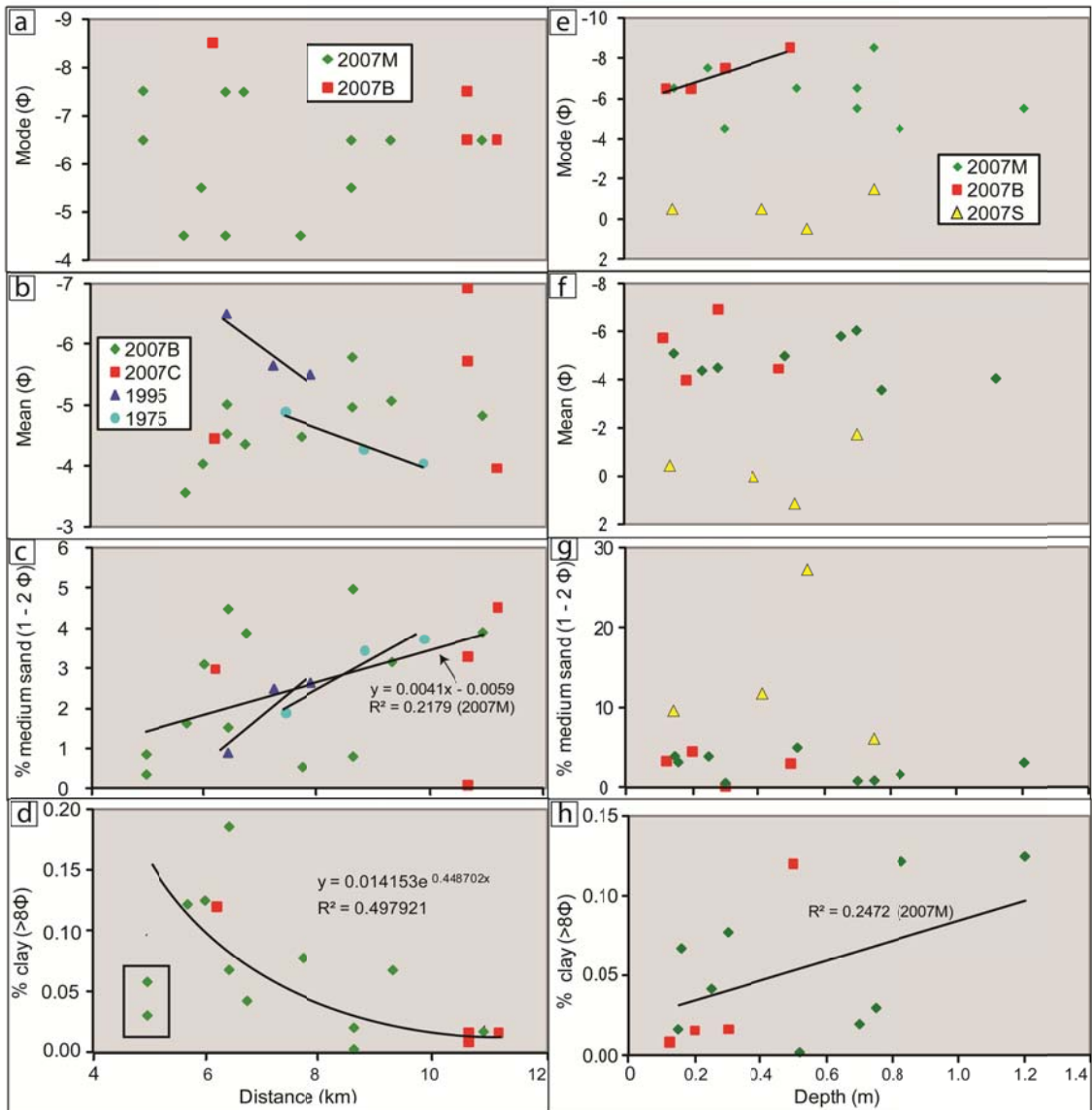
Fig. 8 Statistical grain size characteristics plotted as a function of distance from source (**a-d**) and depth in the deposit (**e-h**) for 2007M, 2007B, 2007S, 1995, and 1975 deposits. Depth values represent the average of the depth ranges sampled. Trend lines are shown for samples of the same unit (in parentheses). **d** Trend line represents both 2007M and 2007B deposits, except two points in the box because they were collected < 5 km from source, which was a bulking, not a debulking, regime (Manville et al., in review).
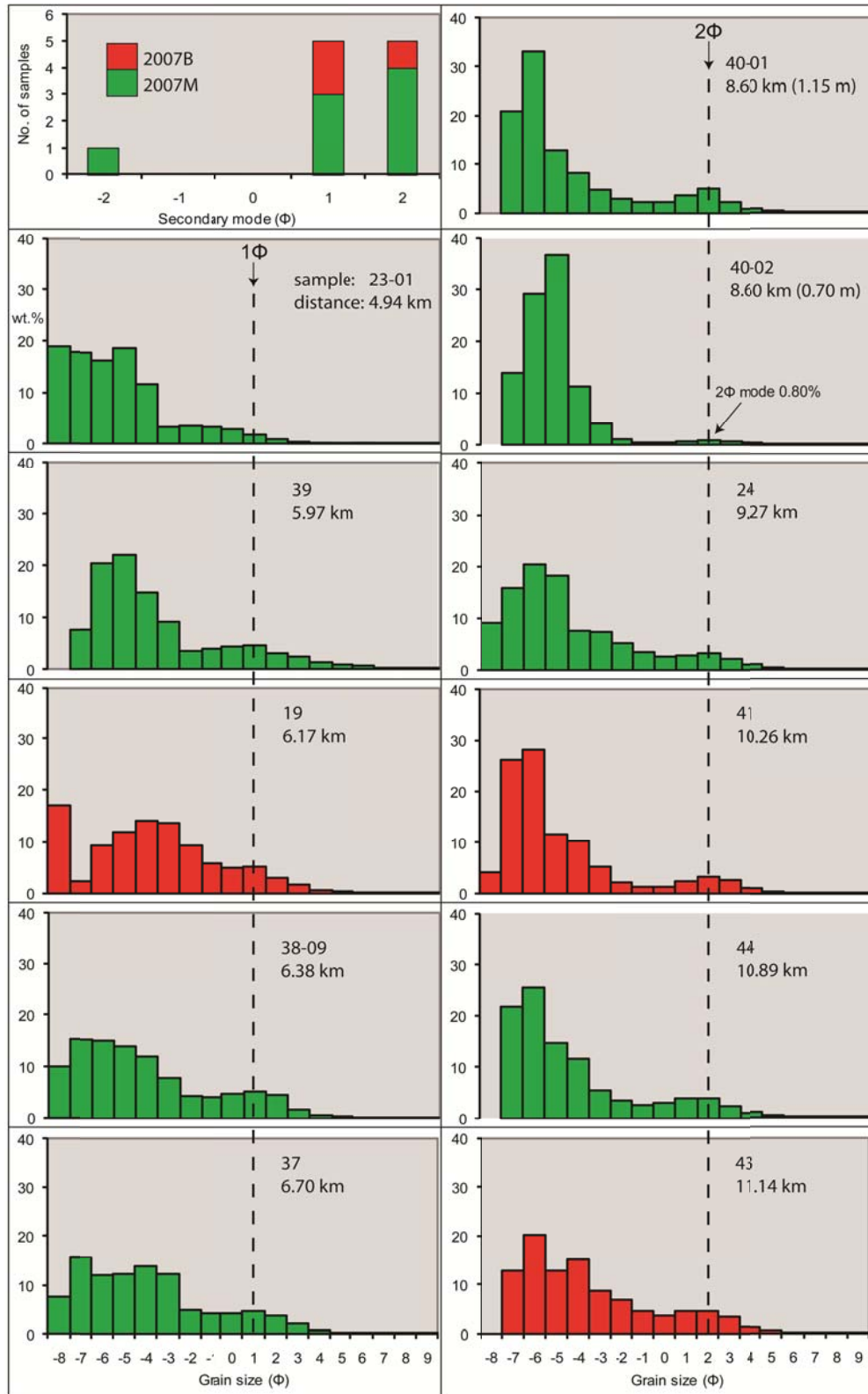
Fig. 9 Histograms of all bimodal grain size distributions in order of distance from Crater Lake with sample number and distance along channel from source. More proximal deposits generally have secondary modes at 1Φ, whereas those of more distal deposits are at 2Φ.

57
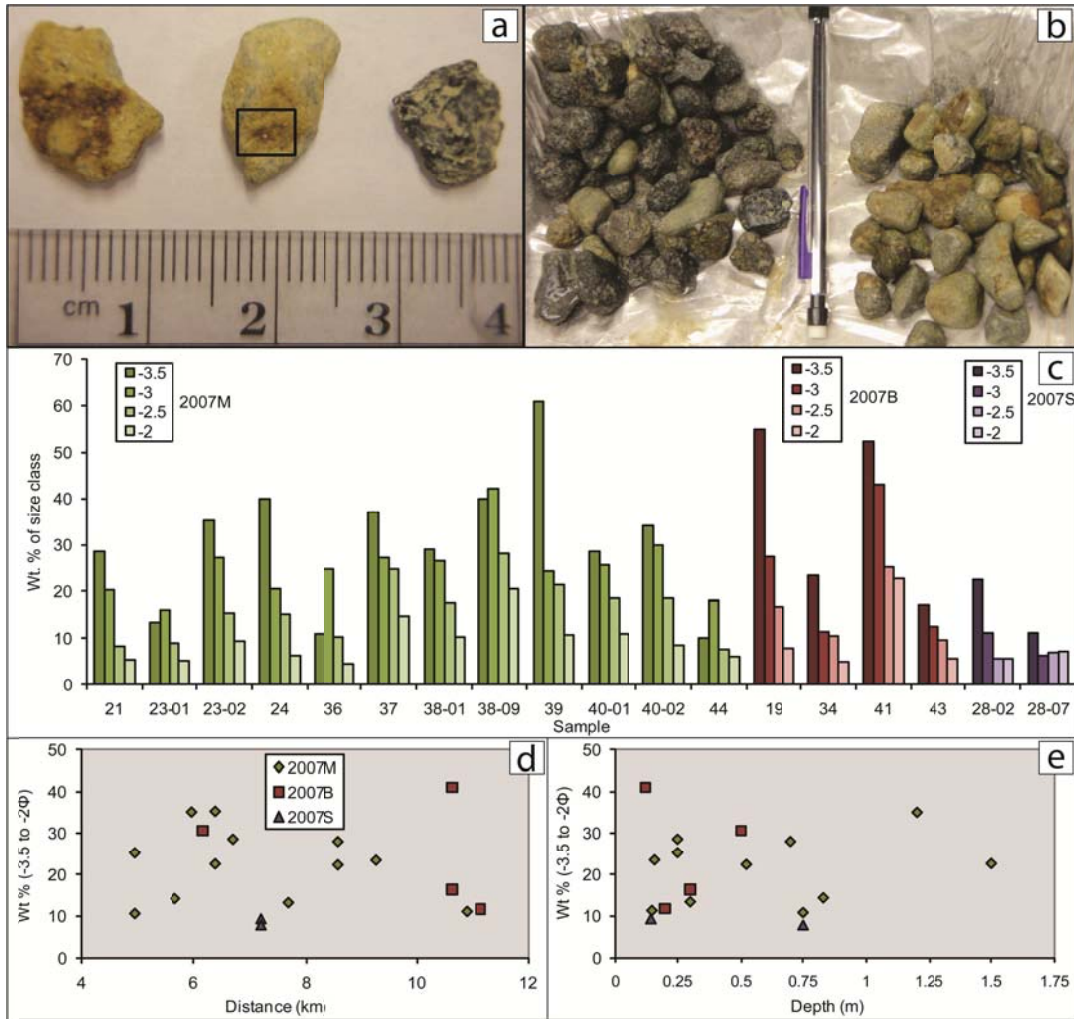
Fig. 10 a Altered clasts with decreasing degree of red alteration from left to right. Left two clasts are classified as altered components due to the presence of red, friable alteration (minimum amount for "altered" classification boxed on second grain). The right has no alteration and has greater angularity and roughness. **b** Clasts (-3.5Φ size class) classified as unaltered (left) and altered (right). Note that some clasts in left category are distinctly rounder and smoother than other unaltered clasts. **c** Weight percentages of altered components of 4 size classes for 2007 samples. All samples are represented except samples 28-04 and 28-05, which had insufficient clasts in the largest size class. **d** Variation in the proportion of altered clasts among samples as a function of distance and **e** as a function of depth in the deposit.
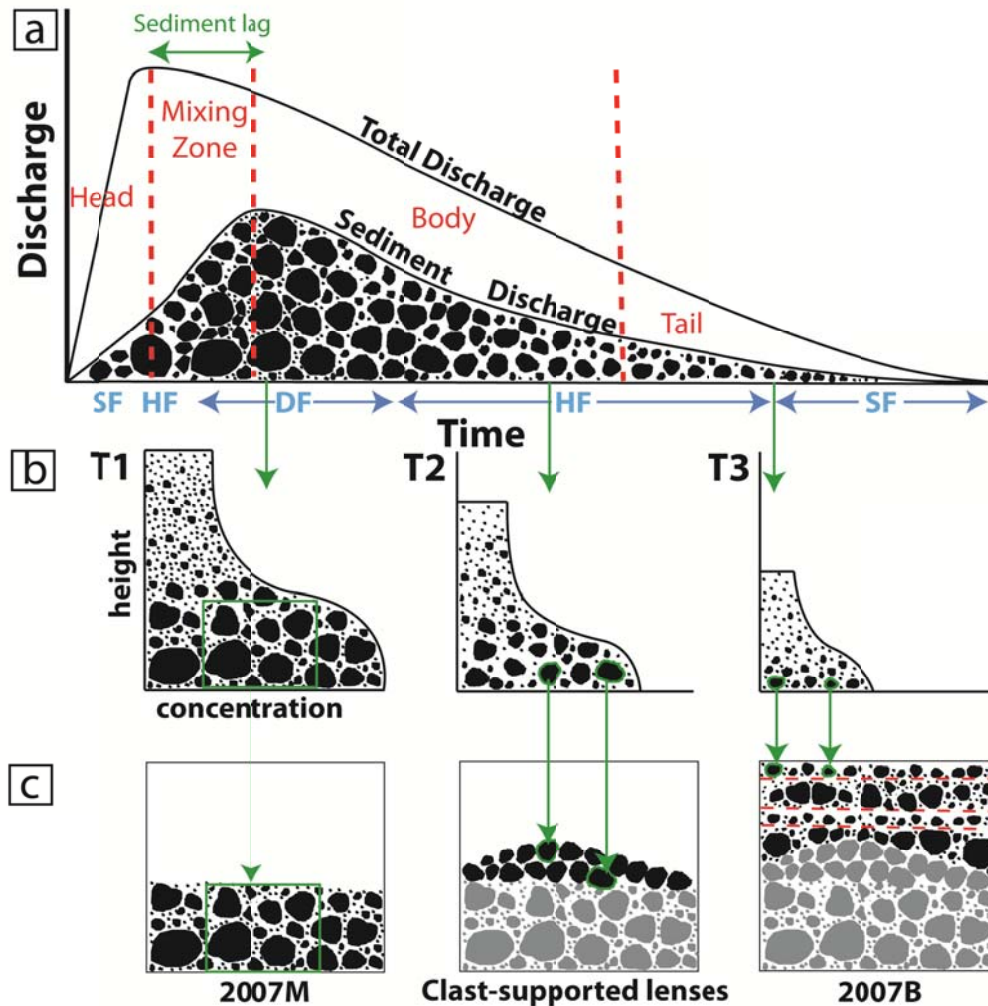
Fig 11a Schematic representation of total discharge and sediment discharge as a function of time for the 18 March 2007 lahar. The proportion of the vertical profile covered by sediment discharge indicates the sediment concentration by volume. SF = streamflow, HF = hyperconcentrated flow, DF = debris flow. Sediment lag indicates the duration between peak total discharge and peak sediment discharge. Relative maximum clast sizes and grain size distributions of the basal flow fine with distance, although the maximum sand abundance is generated through abrasion and cataclasis during peak sediment concentration when collisions between clasts are of the highest magnitude and frequency.

b Sediment concentrations and grain size distributions as a function of height of the flow at successive times during flow evolution. The coarsest clasts are in the depositional basal flow, while fines dominate the transport region.

c Three deposit types (in black) controlled by the density-driven depositional style. 2007M deposits are emplaced by capacity-limited, non-selective vertical accretion, which most closely resembles the character of the basal flow. Clast-supported lenses are interbedded within and above 2007M deposits and represent selective competence-limited deposition, which emplaces the largest, lowest clasts of the basal flow. 2007B deposits are emplaced by primary deposition of thin stratified beds of finer clasts, representing the waning competence of the lahar tail, in addition to reworking of earlier coarser deposits.
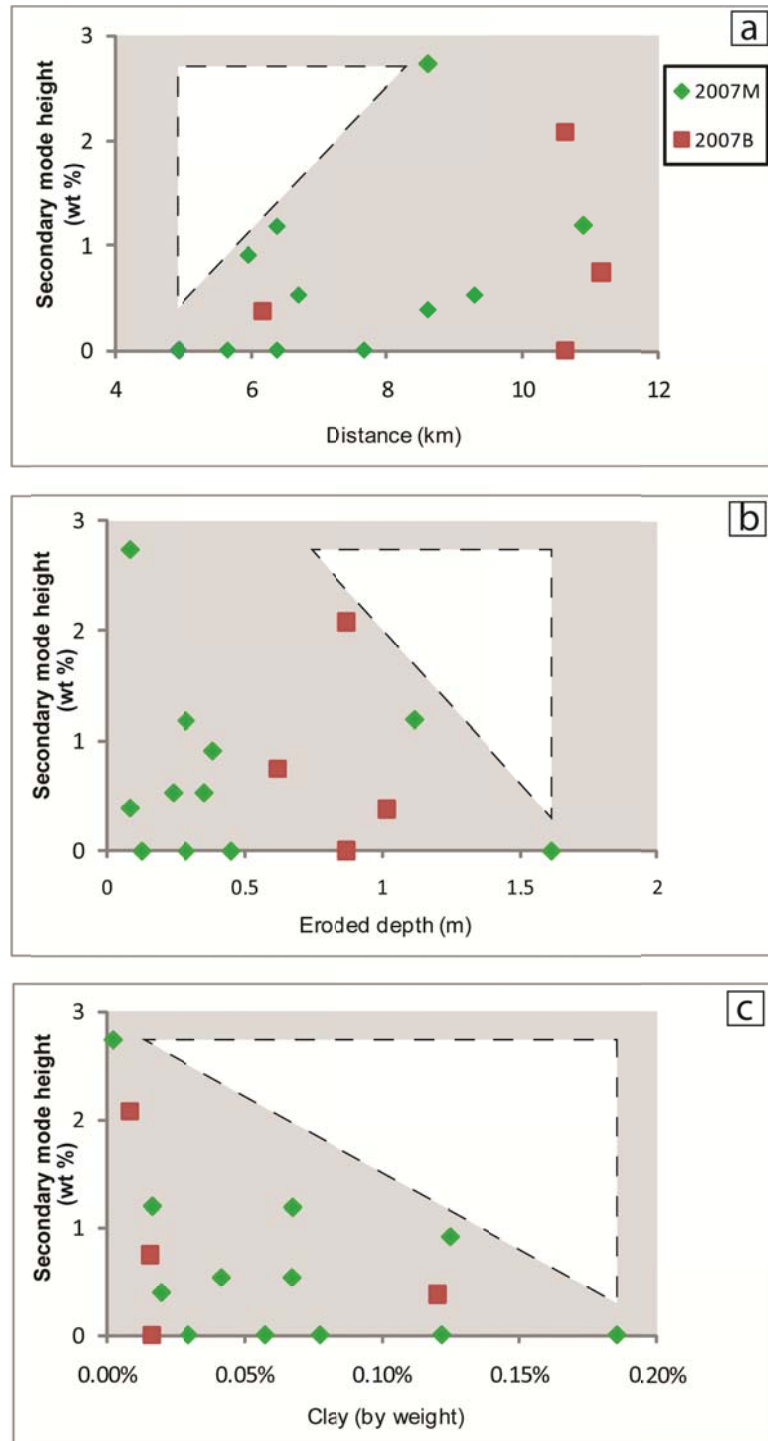
Fig. 12 Heights of 1Φ and 2Φ secondary modes (calculated as the difference between the weight % of the secondary mode and coarser-grained trough) **a** increase with parameters associated with decreased bulking, and **b and c** decrease with parameters associated with increased bulking. Triangular voids show the expected absence of high secondary mode heights for the low or high values associated with increased bulking of external sediment. (V. Manville unpublished eroded depth data)

REFERENCES

Arboleda, R.A., Martinez, M.M.L., 1996. 1992 lahars in the Pasig-Potrero River system. In: Newhall, C.G., Punongbayan, R.S. (Eds.), Fire and Mud, Eruption and Lahars of Mount Pinatubo, Philippines. University of Washington Press, Seattle, pp. 1045-1052.

Baker, V.R., Ritter D.F., 1975. Competence of rivers to transport coarse bedload material. Geological Society of America Bulletin 86, 975-978.

Beverage, J.P., Culbertson, J.K., 1964. Hyperconcentrations of suspended sediment. Journal of the Hydraulics Division, Proceedings of the American Society of Civil Engineers 90, 117-128.

Bradley, W.C., 1970. Effect of weathering on abrasion of granitic gravel, Colorado River (Texas). Geological Society of America Bulletin 81, 61-80.

Bradley, J.B., 1986. Hydraulics and bed material transport at high fine suspended sediment concentrations. Ph.D. dissertation, Colorado State University, Fort Collins.

Capra, L., Poblete, M.A., Alvarado, R., 2004. The 1997 and 2001 lahars of Popocatépetl volcano (Central Mexico): textural and sedimentological constraints on their origin and hazards. Journal of Volcanology and Geothermal Research 131, 351-369.

Carrivick, J.L., Manville, V., Cronin, S.J., 2009. A fluid dynamics approach to modeling the 18th March 2007 lahar at Mt. Ruapehu, New Zealand. Bulletin of Volcanology 71, 153-169.

Castruccio, A., Clavero, J., Rivera, A., 2010. Comparative study of lahars generated by the 1961 and 1971 eruptions of Calbuco and Villarrica volcanoes, Southern Andes of Chile. Journal of Volcanology and Geothermal Research 190, 297-311.

Cheel, R.J., Middleton, G.V., 1986. Horizontal laminae formed under upper flow regime plane bed conditions. Journal of Geology 94, 489-504.

Christensen, B.W., Wood, C.P., 1993. Evolution of a vent-hosted hydrothermal system beneath Ruapehu Crater Lake, New Zealand. Bulletin of Volcanology 55, 547-565.

Costa, J.E., 1983. Paleohydraulic reconstruction of flash-flood peaks from boulder deposits in the Colorado Front Range. Geological Society of America Bulletin 994, 986-1004.

Costa, J.E. 1988. Rheologic, geomorphic, and sedimentologic differentiation of water floods, hyperconcentrated flows, and debris flows. In: Patton, P.C. (Ed.), Flood Geomorphology. John Wiley, Hoboken, NJ, pp. 113-121.

Cronin, S.J., Neall, V.E., 1997. A late Quaternary stratigraphic framework for the northeastern Ruapehu and eastern Tongariro ring plains, New Zealand. New Zealand Journal of Geology and Geophysics. 40, 185-197.

Cronin, S.J., Neall, V.E., Lecointre, J.A., Palmer, A.S., 1996. Unusual "snow slurry" lahars from Ruapehu volcano, New Zealand, September 1995. Geology 24, 1107-1110.

Cronin, S.J., Hodgson, K.A., Neall, V.E., Palmer, A.S., Lecointre, J.A., 1997a. 1995 Ruapehu lahars in relation to the late Holocene lahars of Whangaehu River, New Zealand. New Zealand Journal of Geology and Geophysics 40, 507-520.

Cronin, S.J., Neall, V.E., Lecointre, J.A., Palmer, A.S., 1997b. Changes in Whangaehu river lahar characteristics during the 1995 eruption sequence, Ruapehu volcano, New Zealand. Journal of Volcanology and Geothermal Research 76, 47-61.

Cronin, S.J., Neall, V.E., Lecointre, J.A., Palmer, A.S., 1999. Dynamic interactions between lahars and stream flow: A case study from Ruapehu volcano, New Zealand. Geological Society of America Bulletin 111, 28-39.

Donoghue, S.L., Neall, V.E., Palmer, A.S., Stewart, R.B., 1997. The volcanic history of Ruapehu during the past 2 millenia based on the record of Tufa Trig tephra. Bulletin of Volcanology 59, 136-146.

Fagents, S. A., Baloga, S.M., 2006. Toward a model for the bulking and debulking of lahars. Journal of Geophysical Research 111, B10201, doi:10.1029/2005JB003986, 2006.

Fagents, S.A., Baloga, S.M., 2005. Calculation of lahar transit times using digital elevation data, Journal of Volcanology and Geothermal Research 139, 135-146.

Fahnestock, R.K., Haushild,W.L., 1962. Flume studies of the transport of pebbles and cobbles on a sand bed. Geological Society of America Bulletin 73, 1431-1436.

Fisher, R.V., 1971. Features of coarse-grained, high concentration fluids and their deposits. Journal of Sedimentary Petrology 41, 916-927.

Fisher, R.V., 1983. Flow transformations in sediment gravity flows. Geology 11, 273-274.

Folk, R.L., Ward, W.C., 1957. Brazos River bar: a study in the significance of grain size parameters. Journal of Sedimentary Petrology 27, 3-26.

Goshal K., Mazumder, B.S., 2005. Sediment-induced stratification in turbulent open-channel flow. Environmetrics 16, 673-686.

Graettinger, A.H., 2007. Depositional record of historic lahars in the Whangaehu Gorge, Mt. Ruapehu. Master's Thesis, University of Waikato, New Zealand.

Graettinger, A.H., Manville V., Briggs, R.M., 2010. Depositional record of historic lahars in the upper Whangaehu Valley, Mt. Ruapehu, New Zealand: implications for trigger mechanisms, flow dynamics and lahar hazards. Bulletin of Volcanology 72, 279-296.

Hackett, W.R., Houghton, B.F., 1989. A facies model for a Quaternary andesitic composite volcano: Ruapehu, New Zealand. Bulletin of Volcanology 51, 51-68.

Hancox, G., 2002. Report on sediment availability for lahar bulking in the upper Whangaehu River, Mt. Ruapehu. Department of Conservation client report. 14 pp.

Hancox, G. T., Keys, H., Webby, M.G., 2001. Assessment and mitigation of dam-break lahar hazards from Mt Ruapehu Crater Lake following the 1995-96 eruptions. Paper presented at Engineering and Development in Hazardous Terrains, New Zealand Geotechnical Society, New Zealand Institute of Professional Engineers, Christchurch, New Zealand.

Hanes, D.M., Bowen, A.J., 1985. A granular-fluid model for steady intense bedload transport. Journal of Geophysical Research 90, 9149-9158.

Hiscott, R.N., 1994. Traction-carpet stratification in turbidites–fact or fiction? Journal of Sedimentary Petrology A64, 204-208.

Hodgson, K.A., Manville, V., 1999. Sedimentology and flow behavior of a rain-triggered lahar, Mangatoetoenui Stream, Ruapehu volcano, New Zealand. Geological Society of America Bulletin 111, 743-754.

Hodgson, K.A., Lecointre J., Neall, V.E., 2007. Onetapu Formation: the last 2000 yrs of laharic activity at Ruapehu volcano, New Zealand. New Zealand Journal of Geology and Geophysics 50(2), 81-99.

Iverson, R.M., 1997. The physics of debris flows. Reviews of Geophysics 35, 245-296.

Iverson, R.M., 2005. Debris-flow mechanics. In: Jakob, M., Hungr, O., (Eds.), Debris-flow Hazards and Related Phenomena. Praxis–Springer, Berlin, pp. 103-134.

Iverson, R.M., Vallance, J.W., 2001. New views of granular mass flows. Geology 29, 115-118.

Jerolmack, D.J., Brzinski, T.A., 2010. Equivalence of abrupt grain-size transitions in alluvial rivers and eolian sand seas: A hypothesis. Geology 38, 719-722.

Joyce, K.E., Samsonov, S., Manville, V., Jongens, R., Graettinger, A., Cronin, S.J., 2009. Remote sensing data types and techniques for lahar path detection: A case study

at Mt Ruapehu, New Zealand. Remote Sensing of the Environment 113, 1778-1786.

Kastl, B.C., Manville, V. (in review). Hazards from failures of hydrothermally altered volcanic slopes. Bulletin of Volcanology.

Kodama, Y. 1994. Downstream changes in the lithology and grain size of fluvial gravels, the Watarase River, Japan: Evidence of the role of abrasion in downstream fining. Journal of Sedimentary Research A64, 68-75.

Krumbein, W.C., Pettijohn, F.J., 1938. Manual of Sedimentary Petrography. Appleton-Century-Crofts, New York.

Larcher, M., Fraccarollo, L., Armanini, A., Capart, H., 2007. Set of measurement data from flume experiments on steady uniform debris flows. Journal of Hydraulic Research 45(Extra Issues), 59-71.

Lecointre J., Hodgson, K.A., Neall, V.E., Cronin, S.J., 2004. Lahar-triggering mechanisms and hazard at Ruapehu volcano, New Zealand. Natural Hazards 31, 85-109.

Lube, G., Cronin, S.J., Procter, J.N., 2009. Explaining the extreme mobility of volcanic ice-slurry flows, Ruapehu volcano, New Zealand. Geology 37, 15-18.

Major, J.J., 1997. Depositional processes in large-scale debris-flow experiments. Journal of Geology 105, 345-346.

Major, J. J., Iverson, R.M., 1999. Debris-flow deposition: Effects of pore-fluid pressure and friction concentrated at flow margins. Geological Society of America Bulletin 111(10), 1424-1434.

Major, J.J., 2000. Gravity-driven consolidation of granular slurries: Implications for debris-flow deposition and deposit characteristics. Journal of Sedimentary Research 70, 64-83.

Manville, V., 2004. Palaeohydraulic analysis of the 1953 Tangiwai lahar; New Zealand's worst volcanic disaster. Acta Vulcanologica XVI, 137-152.

Manville, V., Cronin, S.J., 2007. Break-out lahar from New Zealand's Crater Lake. Eos, Transactions American Geophysical Union 88, 441-442.

Manville, V., Hodgson K.A., White, J.D.L., 1998. Rheological properties of a remobilized-tephra lahar associated with the 1995 eruptions of Ruapehu volcano, New Zealand. New Zealand Journal of Geology and Geophysics 41, 157-164.

Manville, V., White, J.D.L., Hodgson, K.A., 2000. Dynamic interactions between lahars and stream flow: A case study from Ruapehu volcano, New Zealand. Geological

Society of America Bulletin 112, 1149-1152.

Manville, V., Hodgson, K.A., Houghton, B.F., Keys, J.R.H., White, J.D.L., 2000. Tephra, snow and water: complex sedimentary responses at an active, snow-capped stratovolcano, Ruapehu, New Zealand. Bulletin of Volcanology 62 278–293.

Manville, V., Graettinger, A., Jongens, R., Cronin, S.J., in review. The 18 March 2007 Crater Lake break-out lahar at Ruapehu, New Zealand. I: geomorphic change and volume balance analysis from airborne LiDAR data. Journal of Geophysical Research.

Massey, C.I., Manville, V., Hancox, G.H., Keys, H.J., Lawrence, C., McSaveney, M., 2009. Out-burst flood (lahar) triggered by retrogressive landsliding, 18 March 2007 at Mt Ruapehu, New Zealand–a successful early warning. Landslides 7, 303-315.

O'Connor, J. E., 1993. Hydrology, hydraulics, and geomorphology of the Bonneville Flood. Geological Society of America. Special paper no. 274, 83 pp.

O'Shea, B.E., 1954. Ruapehu and the Tangiwai disaster. New Zealand Journal of Science and Technology B36, 174-189.

Pearce, T.H., 1971. Short distance fluvial rounding of volcanic detritus. Journal of Sedimentary Petrology 41, 1069-1072.

Pierson, T.C., 1986. Flow behavior of channelized debris flows, Mount St. Helens, Washington. In: Abrahams, A.D. (Ed.), Hillslope Processes. Allen and Unwin, Boston, pp. 269-296.

Pierson, T.C., 1995. Flow characteristics of large eruption-triggered debris flows at snow-clad volcanoes: constraints for debris-flow models. Journal of Volcanology and Geothermal Research 66, 283-294.

Pierson, T.C., 1998. An empirical method for estimating travel times for wet volcanic mass flows. Bulletin of Volcanology 60, 98-109.

Pierson, T.C., 2005a. Hyperconcentrated flow–transitional process between water flow and debris flow. In: Jakob, M., Hungr, O., (Eds.), Debris Flow Hazards and Related Phenomena. Heidelberg, Springer-Praxis, pp. 159-202.

Pierson, T.C., 2005b. Distinguishing between debris flows and floods from field evidence in small watersheds: U.S. Geological Survey Fact Sheet 2004-3142.

Pierson, T.C., Scott, K.M., 1985. Downstream dilution of a lahar: Transition from debris flow to hyperconcentrated streamflow. Water Resoures Research 21, 1511-1524.

Pierson, T.C., Costa, J.C., 1987. A rheologic classification of subaerial sediment-water flows. Geological Society of America Reviews in Engineering Geology 7, 1-12.

Procter, J., Cronin, S.J., Fuller, I.C., Lube, G., Manville, V., 2010. Quantifying the geomorphic impacts of a lake-breakout lahar, Mount Ruapehu, New Zealand. Geology 38, 67-70.

Rădoane, M., Rădoane, N., Durmitriu, D., Miclăus, C., 2008. Downstream variation in bed sediment size along East Carpathian rivers: evidence of the role of sediment sources. Earth Surface Processes and Landforms 33, 674-694.

Rodolfo, K. S., Umbal, J.V., Alonso, R.A., Remotigue, C.T., Paladio-Melosantos, M.L., Salvador, J.H.G., Evangelista, D., Miller, Y., 1996. Two years of lahars on the western flank of Mount Pinatubo: Initiation, flow processes, deposits, and attendant geomorphic and hydraulic changes. In: Newhall, C.G., Punongbayan, R.S. (Eds.), Fire and Mud: Eruptions and Lahars of Mount Pinatubo, Philippines. University of Washington Press, Seattle, pp. 989-1013.

Schmeeckle, M., Nelson, J., Pitlick, J., Bennett, J., 2001. Interparticle collision of natural sediment grains in water. Water Resources Research 37, 2377-2391.

Schumm, S.A., Stevens, M.A., 1973. Abrasion in place: A mechanism for rounding and size reduction of course sediments in rivers. Geology 1, 37-40.

Scott, K.M., 1988. Origins, behavior, and sedimentology of lahars and lahar-runout flows in the Toutle-Cowlitz River System. U.S. Geological Survey Professional Paper 1447-A, Washington, DC, pp. 1-74.

Scott, K.M., Vallance, J.W., Pringle, P.T., 1995. Sedimentology, behavior, and hazards of debris flow at Mount Rainier, Washington. U.S. Geological Survey Professional Paper 1547, 106.

Smith, G.A., 1986. Coarse-grained nonmarine volcaniclastic sediment: Terminology and depositional processes. Geological Society of America Bulletin 97, 1-10.

Sohn, Y.K., 1997. On traction-carpet sedimentation. Journal of Sedimentary Research 67, 502-509.

Stevens, N.F., Manville, V., Heron, D.W., 2002. The sensitivity of a volcanic flow model to digital elevation model accuracy: Experiments with digitized map contours and interferometric SAR at Ruapehu and Taranaki volcanoes, New Zealand. Journal of Volcanology and Geothermal Research 119, 89-105.

Vallance, J.W., 1994. Experimental and field studies related to the behavior of granular mass flows and the characteristics of their deposits. Ph.D. Dissertation, Michigan Techological University, Houghton, MI.

Vallance, J.W., 2000. Lahars. In: Sigurdsson, H. (Ed.) Encyclopedia of Volcanoes. Elsevier, New York, pp. 601– 616.

Vallance, J.W., Scott, K.M., 1997. The Osceola Mudflow from Mount Rainier: Sedimentology and hazard implications of a huge clay-rich debris flow. Geological Society of America Bulletin 109, 143-163.

Walton, A.W., Palmer, B.A., 1988. Lahar facies of the Mount Dutton Formation (Oligocene-Miocene) in the Marysvale Volcanic Field, southwestern Utah. Geological Society of America Bulletin 100, 1078-1091.

Weirich, F. H., 1989. The generation of turbidity currents by subaeriel debris flows, California. Geological Society of America Bulletin 101, 278-291.